# Arctic Ocean Simulations in the CMIP6 Ocean Model Intercomparison Project (OMIP)

Qi Shu[1,2,3], Qiang Wang[4], Chuncheng Guo[5], Zhenya Song[1, 2, 3], Shizhu Wang[1, 2, 3], Yan He[1, 2, 3], Fangli Qiao[1, 2, 3]

[1]First Institute of Oceanography, and Key Laboratory of Marine Science and Numerical Modeling, Ministry of Natural Resources, Qingdao, 266061, China
[2]Laboratory for Regional Oceanography and Numerical Modeling, Pilot National Laboratory for Marine Science and Technology, Qingdao, 266067, China
[3]Shandong Key Laboratory of Marine Science and Numerical Modeling, Qingdao, 266061, China
[4]Alfred Wegener Institute Helmholtz Centre for Polar and Marine Research (AWI), Bremerhaven, 27570, Germany
[5]NORCE Norwegian Research Centre, Bjerknes Centre for Climate Research, Bergen, 5007, Norway

*Correspondence to*: Qi Shu (shuqi@fio.org.cn)

**Abstract.** Arctic Ocean simulations in 19 global ocean-sea ice models participating in the Ocean Model Intercomparison Project (OMIP) of the CMIP6 are evaluated in this paper. Our results indicate that no significant improvements were achieved in the Arctic Ocean simulations from the previous Coordinated Ocean-ice Reference Experiments phase II (CORE-II) to the current OMIP. Large model biases and inter-model spread exist in the simulated mean state of the halocline and Atlantic Water layer in the OMIP models. Most of the OMIP models suffer from too thick and deep Atlantic Water layer, too deep halocline base, and large fresh biases in the halocline. The OMIP models largely agree on the inter-annual and decadal variability of the Arctic Ocean freshwater content and volume/heat/freshwater transports through the Arctic Ocean gateways. The models can reproduce observed changes in volume, heat and freshwater transports through the gateways except for the Bering Strait. Overall, the performance of the Arctic Ocean simulations is similar between the CORE2-forced OMIP-1 and JRA55-do-forced OMIP-2.

## 1 Introduction

As the northernmost ocean on Earth, the Arctic Ocean is of great concern to researchers and the general public, especially under the background of the global warming. The decline of Arctic sea ice and warming of the water in the Arctic Ocean indicate that the Arctic Ocean has been experiencing rapid climate change (Onarheim et al., 2018; Stroeve and Notz, 2018; Polyakov et al., 2012, 2017; Danielson et al., 2020). The Arctic Ocean is projected to warm faster than global ocean average, a phenomenon called Arctic Ocean amplification (Shu et al., 2022). The changes of the Arctic Ocean potentially affect the climate system beyond the Arctic. For example, the sea ice decline in the Arctic tends to cause cold winters and extreme weather events over the mid-latitude continents in the Northern Hemisphere (Li et al., 2020; Outten and Esau, 2012; Kim et al., 2014; Cohen et al., 2020), and the storage and release of freshwater from the Arctic Ocean can influence the large scale

ocean circulation by freshening the upper North Atlantic ocean (Jungclaus et al., 2005; Goosse et al., 1997; Wadley and Bigg, 2002; Shu et al., 2017; Zhang et al., 2021).

The Arctic Ocean is surrounded by the Eurasian and the North American continents (Fig. 1), which is connected to the
35  Atlantic Ocean on both sides of Greenland and to the Pacific Ocean through the Bering Strait. The general circulation in the Arctic Ocean is the superposition of Atlantic Water flowing into and around the Arctic Basin and two main wind-driven circulation features of the interior stratified Arctic Ocean: the Transpolar Drift Stream and the Beaufort Gyre (Fig. 1) (Timmermans and Marshall, 2020; Wang and Danilov, 2022). Warm and saline Atlantic Water enters the Arctic Ocean with two branches. One branch passes the Fram Strait and supplies the warm AW layer of the Arctic Ocean (Våge et al., 2016;
40  Beszczynska-Möller et al., 2012; Rudels et al., 2015). The other enters the Barents Sea and then Kara Sea and finally flows to the surface, intermediate and deeper layers of the Arctic Ocean (Karcher, 2002; Schauer et al., 2002; Maslowski et al., 2004). The Atlantic Water circulates mainly cyclonically along the peripheries of the Arctic basins and is aligned with the continental slope (Karcher et al., 2003; Timmermans and Marshall, 2020). Fresh Pacific Water flows into the Arctic Ocean through the Bering Strait (Woodgate, 2018b; Woodgate and Peralta-Ferriz, 2021), and leaves the Arctic via the Fram Strait
45  and Canadian Arctic Archipelago (Hu et al., 2019; Steele et al., 2004; Lique et al., 2010; Wang et al., 2021).

The Arctic Ocean is a large freshwater reservoir, which plays a critical role in the global climate system. Ekman convergence associated with the Arctic atmospheric anticyclonic circulation centered in the Beaufort Gyre region leads to high liquid freshwater content in the Arctic Ocean (Proshutinsky et al., 2009, 2002). The Arctic Ocean receives large amounts of fresh water from river runoff, oceanic freshwater flux through Bering Strait, and net precipitation, and releases fresh water through
50  Davis Strait and Fram Strait (Serreze et al., 2006; Dickson et al., 2007; Ilicak et al., 2016). Observations show that liquid freshwater stored in the Arctic Ocean has increased since the mid-1990s and stabilized in the 2010s with an unprecedented amount of freshwater accumulated in the Amerasian Basin (Rabe et al., 2014; Polyakov et al., 2013; Wang et al., 2019b; Wang and Danilov, 2022; Solomon et al., 2021).

Water masses in the Arctic Ocean can be distinguished with five separate layers (Rudels, 2009), including a ~50-m-thick
55  upper polar mixed layer, a 100–250-m-thick halocline layer, a 400–700-m-thick Atlantic layer, an intermediate layer below the Atlantic layer, and a bottom-most layer containing deep and bottom waters. Since the 1990s significant warming signals have been observed in the upper polar mixed layer and Atlantic Water layer (Polyakov et al., 2012, 2020a; Ingvaldsen et al., 2021; Li et al., 2022; Steele et al., 2008), together with a weakening of cold halocline layer and an increase of upward oceanic heat flux of Atlantic layer in the eastern Arctic Ocean (Polyakov et al., 2020c).

60  Ocean/sea-ice and climate models are often used for scientific studies on the Arctic Ocean due to the limited amount of observational data under the harsh environmental conditions. To validate and further improve model performances in the Arctic Ocean, the Arctic Ocean Model Intercomparison Project (AOMIP) and Forum for Arctic Modeling and Observational Synthesis (FAMOS) were initiated in 1999 and 2013 (Proshutinsky et al., 2001, 2016), respectively. Significant progresses have been made in AOMIP and FAMOS, for example, some systematic biases in Arctic Ocean models have been identified

and some related solutions have been recommended (Holloway et al., 2007; Golubeva and Platov, 2007; Zhang and Steele, 2007; Proshutinsky et al., 2007; Aksenov et al., 2016; Hu et al., 2019).

Focusing on the global scale ocean simulations, the Coordinated Ocean-ice Reference Experiments (COREs) and subsequent Ocean Model Intercomparison Project (OMIP) proposed by the WCRP (World Climate Research Programme)/CLIVAR (Climate and Ocean: Variability, Predictability and Change) Working Group on Ocean Model Development were also successively initiated (Griffies et al., 2009, 2012, 2016). COREs and OMIP aim to provide a framework for evaluating, understanding, and improving the ocean and sea-ice components of global climate and Earth system models contributing to the Coupled Model Intercomparison Project (CMIP). OMIP is an endorsed project in CMIP Phase 6 (CMIP6). The performances of COREs phase II (CORE-II) models in simulating Arctic sea ice, liquid freshwater, hydrography, and volume/heat/freshwater fluxes were comprehensively assessed (Wang et al., 2016a, b; Ilicak et al., 2016). Arctic sea ice simulations by the recent OMIP models were also evaluated by Tsujino et al. (2020). However, Arctic Ocean simulations by the OMIP ocean models, most of which were used as the ocean components of the fully-coupled models in CMIP6, have not been evaluated.

In this work we analyse the Arctic Ocean properties simulated by the models participating in the CMIP6 OMIP to evaluate the latest ocean components of CMIP6 climate models in the Arctic Ocean. This work is to some extent an update of Wang et al. (2016a, b) and Ilicak et al. (2016), with one of the aims to examine if some progresses in simulating the Arctic Ocean have been made in the global ocean and sea ice models, from the previous CMIP5 phase to the most recent CMIP6 phase.

Ocean-sea ice models participating in the CMIP6 OMIP are driven by the specified common atmosphere forcing data sets. Their initial conditions of temperature and salinity are observational-based climatology from World Ocean Atlas 2013 (Locarnini et al., 2013; Zweng et al., 2013). Two versions of OMIP experiments were proposed in the framework of CMIP6, the version driven by the CORE2 forcing (OMIP-1) and the version driver by the JRA55-do forcing (OMIP-2). The CORE2 forcing contains the inter-annually varying atmospheric forcing and river runoff during 1948 to 2009 (Large and Yeager, 2009), which have been developed from the National Centers for Environmental Prediction/National Center for Atmospheric Research (NCEP/NCAR) reanalysis and the observation-based runoff data provided by Dai and Trenberth (2002) and Dai et al. (2009). The forcing is the same as that in the CORE-II project. The temporal frequency and horizontal resolution in CORE2 forcing are 6h and 1.875 °, respectively. The JRA55-do forcing used in OMIP-2 (Tsujino et al., 2018) is based on the Japanese Reanalysis (JRA-55) product from Kobayashi et al. (2015). For OMIP-2 simulations, JRA55-do forcing covers 1958 to 2018. It has higher temporal frequency (3 h) and refined horizontal resolution (0.5625 °) compared to CORE2 forcing. In this study, the Arctic Ocean simulations from 19 ocean-sea ice models (Table 1) participating in OMIP-1 and/or OMIP-2 experiments are evaluated. 8 models, including AWI-CM-1-1-LR, CESM2, CMCC-CM2-SR5, EC-Earth3, FGOALS-f3-L, MIROC6, MRI-ESM2-0, and NorESM2-LM, provide both OMIP-1 and OMIP-2 simulations, which offer an opportunity to study the simulation differences related to forcing. Based on the OMIP protocol, each model should run for no less than five cycles of the forcing periods (1948–2009 for OMIP-1 and 1958–2018 for OMIP-2) to provide a model state that does not

drift much anymore. Here we mainly focus on the last cycle of each model to study the model performances in the Arctic Ocean.

100 The Arctic Ocean in this study refers to the Arctic Basin (Eurasian and Amerasian basins) and its surrounding shelf seas, including the Barents, Kara, Laptev, East Siberian, Chukchi, and Beaufort seas, as well as Baffin Bay (Fig. 1). Using this definition, the four gateways, including Bering Strait, Fram Strait, Barents Sea Opening (BSO), and Davis Strait (Fig. 1), can be conveniently used to study the volume, heat and freshwater exchanges between the Arctic Ocean and lower-latitude oceans.

105 This paper is organized as follows. Section 2 shows evaluation results, including the evaluation of mean hydrography, liquid freshwater content, changes in Atlantic Water layer, stratification, and gateway transports. Section 3 provides a summary and conclusions.

## 2 Results

We mainly evaluate OMIP simulated climatology and changes of Arctic Ocean hydrography, liquid freshwater content,
110 mixed layer depth, cold halocline base depth, and gateway transports, using the PHC3.0 climatology (Steele et al., 2001) and other relevant observations from published literatures.

### 2.1 Mean Hydrography

The PHC3.0 climatology is mainly based on observations before 2000, so the period 1971-2000 was chosen to evaluate the models. The PHC3.0 climatology shows that the Arctic basin-mean temperature is cold in the surface and deep/bottom layers,
115 and relatively warm in the Atlantic Water layer (Fig. 2). The Atlantic Water layer is mainly located at the depths between 150–900 m with a warm core between 200–400 m and 400–600 m in the Eurasian Basin and Amerasian Basin, respectively. Most models in OMIP-1 and OMIP-2 can reproduce the vertical structures of the temperature but exhibit large biases and inter-model spreads (Fig. 2). Several models, such as CanESM5, CMCC-CM2-SR5, CMCC-ESM2, and NorESM2-LM, cannot reproduce the warm layer, while the warm cores in CAS-ESM2-0, CESM2, FIO-ESM-2-0, and GFDL-CM4 are too
120 warm. AWI-CM-1-1-LR has overall the best performance in representing the vertical temperature profiles in OMIP-1, although its warm core is relatively warm in OMIP-2 simulation. The more realistic simulations in AWI-CM-1-1-LR may have benefited from its relatively high resolution (~24 km) in the Arctic Ocean.

Figure 3a–c shows the PHC3.0 and the multi-model mean potential temperature at 400 m, a depth that was used in previous model intercomparison studies (Ilicak et al., 2016). The eight models providing results for both OMIP-1 and OMIP-2 are
125 used in the calculation of the multi-model mean here. The Atlantic Water layer temperature decreases along the pathways of the Atlantic Water. It is around 2 ℃ near the Fram Strait, and decreases gradually to about 0.8 ℃ near the Lomonosov Ridge and to about 0.4 ℃ in the Canada Basin (Fig. 4a). However, the Atlantic Water layer in both the OMIP-1 and OMIP-2 multi-model mean results is too cold and its warm temperature signal disappears rapidly along the propagation pathway

compared to the observations (Fig. 3b and c), which is similar to that in the CORE-II simulations (Ilicak et al., 2016). The
cold biases may be caused by too weak heat transport from the Fram Strait and too cold temperature in the outflow from the
Eurasian continental shelf through the St. Anna Trough. Figures 2 and 3a–c show that the magnitudes of the Atlantic Water
layer temperature biases are similar in OMIP-1 and OMIP-2.

Another bias in the OMIP models is the too thick Atlantic layer shown by Fig. 4. The observed Atlantic Water layer is
mainly located at 150–900 m depths, while the simulated Atlantic Water layer lower boundary is deeper than 1200 m (Fig.
4b and c). The depth of the highest temperature is also deeper in the models. The too thick and deep Atlantic Water layer,
which is also found in AOMIP and CORE-II simulations (Holloway et al., 2007; Ilicak et al., 2016), is likely the
consequences of too much spurious diapycnal mixing due to low resolution and numerical mixing associated with the
advection operator (Zhang and Steele, 2007; Holloway et al., 2007, Wang et al., 2018). Figures S1 and S2 indicate that the
issue of too thick and deep Atlantic Water layer is common in OMIP models, and some models did not simulate a warm
Atlantic Water layer.

The biases of salinity profile in the Eurasian and Amerasian basins are shown in Fig. 5. For the upper polar mixed layer, both
positive and negative biases are found in both the suites of OMIP models, and the multi-model mean biases are positive in
both the Eurasian and Amerasian Basins in OMIP-1, but is negative in the Amerasian Basin in OMIP-2. The surface salinity
biases in OMIP simulations are similar to that in CORE-II simulations (Ilicak et al., 2016), and are much smaller than those
in CMIP5 and CMIP6 simulations (Shu et al., 2019; Khosravi et al., 2022). This may be related to the sea surface salinity
restoring commonly used in ocean-sea ice models (Wang et al., 2018), which is intended to sustain model stability and to
avoid unbounded local salinity trends that can occur in response to inaccuracies in, for example, precipitation forcing
(Griffies et al., 2009).

Large salinity biases are found in the upper 400-m ocean, and most OMIP models suffer from too fresh biases at subsurface
(50–400 m) (Figs. 3d–f and 5). The maximum biases in OMIP-1 multi-model mean are −0.42 and −0.57 psu in the Eurasian
and Amerasian Basins, respectively. OMIP-2 has relatively larger biases with the largest biases of −0.49 and −0.77 psu in the
Eurasian and Amerasian Basins, respectively. Similar fresh biases are also found in CORE-II, and coupled CMIP5 and
CMIP6 simulations (Ilicak et al., 2016; Shu et al., 2019; Khosravi et al., 2022). It is possibly caused by the absence of proper
parameterization of subgrid scale brine rejection in these models (Ilicak et al., 2016; Nguyen et al., 2009). Different from
most models, EC-Earth3 and IPSL-CM6A-LR have obvious positive salinity biases (larger than 1 psu in the Eurasian Basin)
at subsurface, which has not been found in CORE-II simulations (Ilicak et al., 2016).

Both the simulated temperature and salinity show that OMIP models have large inter-model spread, including the halocline
and Atlantic Water layer (Figs. 2, 5, S1 and S2), which has also been found in AOMIP and CORE-II simulations (Holloway
et al., 2007; Ilicak et al., 2016). The eight models providing results for both OMIP-1 and OMIP-2 indicate that OMIP-2
simulations have relatively smaller inter-model spread than OMIP-1 simulations (Fig. 6). The overall temperature and
salinity biases and inter-model spreads in OMIP simulations are similar to those in CORE-II simulations. It indicates that
there are no significant improvements in Arctic Ocean simulations from CORE-II (CMIP5 phase) to OMIP (CMIP6 phase).

## 2.2 Liquid Freshwater Content

We use 34.8 psu, the mean Arctic salinity (Aagaard and Carmack, 1989), as the reference salinity to calculate liquid
165    freshwater column and freshwater transport, which was commonly used in previous studies (Jahn et al., 2012; Wang et al.,
2016b; Serreze et al., 2006; Haine et al., 2015). The liquid freshwater column (in meter) is calculated as follows:

$$FWC = \int_{-H_{ref}}^{0} (1 - S(z)/S_{ref})dz, \qquad (1)$$

where $S(z)$ is salinity at depth z, $S_{ref}$ is reference salinity, and $H_{ref}$ is the depth where seawater salinity is equal to the
reference salinity. Integrating the freshwater column in an area one gets the volumetric freshwater content.

170    Observations show that liquid freshwater column in the Arctic Ocean is the highest in the Beaufort Gyre because of the
Ekman convergence associated with the atmospheric Beaufort High (Fig. 7a). Both OMIP-1 and OMIP-2 models can
reproduce this spatial pattern (Fig. 7). Consistent with the fresher biases shown in Figs. 5 and 6, OMIP-2 models simulated
more freshwater content in the Arctic Ocean than the observations and OMIP-1 (Figs. 7 and 8). Freshwater storage in the
Arctic basin (where bottom topography is deeper than 500 m) is $55.8 \times 10^3$ km$^3$ based on PHC3.0 climatology, and is
175    $60.5 \times 10^3$ and $66.3 \times 10^3$ km$^3$ in OMIP-1 and OMIP-2 based on the eight models, respectively. OMIP models also have large
inter-model spreads in the freshwater content simulations (Figs. S3 and S4). CMCC-CM2-SR5, CMCC-ESM2, and GFDL-
OM4p5B in OMIP-1 and CMCC-CM2-SR5, CNRM-CM6-1 and MRI-ESM2-0 in OMIP-2 have too much freshwater
content in the Arctic Ocean, while IPSL-CM6A-LR and NorESM2-LM in OMIP-1 have too little freshwater content.

Despite the model spreads in the simulated mean state, OMIP-1 and OMIP-2 models show good agreement on the inter-
180    annual and decadal variability of liquid freshwater content in the Arctic Basin (Fig 8). OMIP simulations indicate a negative
trend in freshwater content in the Arctic Basin from the 1960s to the mid-1990s, and then a positive trend which is consistent
with observations (Rabe et al., 2014; Wang et al., 2019b). An unprecedented amount of freshwater has accumulated in the
Amerasian Basin since the 1990s (Rabe et al., 2014; Polyakov et al., 2013; Wang et al., 2019b; Wang and Danilov, 2022;
Solomon et al., 2021; Proshutinsky et al., 2019). In the last decade (2010s), the Arctic total liquid freshwater content became
185    relatively stable (Solomon et al., 2021), which is also reproduced by OMIP-2 simulations (Fig 8). However, the overall
positive trend since the 1990s in OMIP is relatively weaker than the observations, which was also found in CORE-II
simulations (Wang et al., 2016b).

## 2.3 Changes in Atlantic Water layer

Arctic Ocean Atlantic Water layer temperature varies on different time scales (Polyakov et al., 2004). Its fluctuations are
190    linked to the highly variable nature of the Atlantic Water inflows, with abrupt cooling/warming events (Polyakov et al.,
2020a). A warming pulse was observed in the 1990s in the Eurasian Basin and then in the Amerasian Basin in 2000s (Steele
and Boyd, 1998; Polyakov et al., 2012). It is about 1 ℃ warming in the 1990s compared to 1970s in the Eurasian Basin
based on observations (Polyakov et al., 2020a). Figures 9 and S5 show that OMIP-1 models are able to reproduce a similar
warming pulse, but it is much weaker than the observations. In OMIP-2 simulations, the warming pulse in the Eurasian

195  Basin is also much weaker than the observed (Figs. 9 and S6). No decadal warming averaged in the Amerasian Basin in the 1990s is present in both the OMIP multi-model means (Fig 9). The model spreads are large, with some models being able to reproduce the decadal variability and some models not (Figs. S5 and 6).

Polyakov et al. (2020a) found that the Atlantic Water layer temperature increased rapidly in the 2000s, and then reached a temporary quasi-equilibrium afterwards. The rapid Atlantic Water layer warming in this period can be simulated by OMIP-2

200  models, which cover the last decade in the simulations. However, in both OMIP-1 and OMIP-2, the rapid Atlantic Water layer warming in the 2000s is not as prominent as found in observations (Figs. 9 and S5).

The agreement on the inter-annual and decadal variability of Atlantic Water layer temperature in OMIP-1 and OMIP-2 is lower than liquid freshwater content (Figs. 8 and 9). One reason is the significant influence of the remarkable warming at the end of the preceding simulation cycle on the following cycle, which is more pronounced in OMIP-2 because the temperature

205  is higher in 2018 than in 2009 (the years that were used to initialize new simulation cycles in OMIP-2 and OMIP-1, respectively). All the OMIP-2 models show a strong warm signal in the first two decades (Fig S6), indicating that the re-initialization can have impacts for at least two decades. A warm episode developed in the 1960s in the Amerasian Basin in OMIP-2 because the high temperature in the Eurasian Basin inherited from the preceding simulation cycle propagated downstream into the Amerasian Basin (Fig 9d).

## 2.4 Stratification

To evaluate the ocean stratification, we compared surface mixed layer depth and cold halocline base depth with the observations in Figs. 10 and 11. Mixed layer depth is important for Arctic physical, chemical and biological processes (Peralta-Ferriz and Woodgate, 2015). In this study, it is defined as the depth where the potential density is larger than the surface potential density by 0.1 $kg/m^3$, which is considered a suitable threshold criterion for calculating surface mixed layer

215  depth in the Arctic Ocean (Peralta-Ferriz and Woodgate, 2015). Arctic Ocean mixed layer depth shows a remarkable seasonal cycle, and it is deep in winter and shallow in summer. Considering that the summer mixed layer depth in many areas of the Arctic Ocean is ~10 m based on observations (Peralta-Ferriz and Woodgate, 2015), which is quite close to the thickness of the first vertical layer in many OMIP models, we only study mixed layer depth in winter in this paper.

Using the observations during 1979–2012, Peralta-Ferriz and Woodgate (2015) quantified Arctic Ocean surface mixed layer

220  depth by dividing the Arctic Ocean into six regions (Southern Beaufort Sea, Canada Basin, Chukchi Sea, Makarov Basin, Eurasian Basin and Barents Sea), and their estimate shows that cold season (November–May) mixed layer depths in these six regions are 29.0, 33.1, 34.6, 52.0, 72.5, and 168 m, respectively. So mixed layer depth is deepest in the Barents Sea, followed by the Eurasian Basin and Makarov Basin, and is relatively shallow in the southern Beaufort Sea, the Canadian Basin and the Chukchi Sea. Figure 10 shows that both the OMIP-1 and OMIP-2 multi-model mean results can reproduce this

225  spatial pattern. However, the simulated mixed layer depth in the Eurasian Basin is shallower than the observations, especially in the OMIP-1 experiments. Figures S7 and S8 indicate that both OMIP-1 and OMIP-2 models have quite large

inter-model spreads in the simulated mixed layer depth, which is similar to that in the CORE-II simulations (Ilicak et al., 2016).

The Arctic cold halocline layer is an important insulator between the warm Atlantic Water layer and the cold surface mixed
230  layer. The cold halocline base depth used here is defined as the depth where the ratio of the density gradient due to temperature to the density gradient due to salinity equals 0.05 (Bourgain and Gascard, 2011), that is:

$$R_\rho = (\alpha\, \partial\theta/\partial z)/(\beta\, \partial S/\partial z) = 0.05, \tag{2}$$

where $\alpha$, $\beta$, $\theta$, and S are the thermal expansion coefficient, haline contraction coefficient, potential temperature and salinity, respectively. This depth characterizes the transition from halocline to thermocline (Bourgain and Gascard, 2011).

235  The Arctic cold halocline base depth derived from the PHC3.0 climatology and OMIP simulations are shown in Fig. 11. It is shallow in the Eurasian Basin and deep in the Amerasian Basin according to PHC3.0 (Fig. 11a), and this feature can be reproduced by OMIP models (Fig. 11b and c). However, the simulated halocline base depth is too deep in both the Eurasian and Amerasian Basins. In most area of the Eurasian Basin, it is shallower than 100 m based on PHC3.0, but it is deeper than 120 m in the OMIP simulations. It is shallower than 210 m based on PHC3.0 in the Canada Basin, while it is deeper than 300
240  m in the OMIP simulations. The inter-model spreads are also quite large in both OMIP-1 and OMIP-2 models (Figs. S9 and S10). AWI-CM-1-1-LR in OMIP-2 performs the best out of all models. Surface mixed layer depth in AWI-CM-1-1-LR also fits the observations well (Fig. S8). So, AWI-CM-1-1-LR in OMIP-2 has a good performance in the stratification simulations. Observations indicate that the cold halocline layer in the Eurasian Basin has a thinning trend recently (Polyakov et al., 2020c, b). This trend can be reproduced by OMIP-2 multi-model mean result (Fig. 11d) and each OMIP-2 individual model (not
245  shown). OMIP-2 multi-model mean result also shows the cold halocline base depth in the Amerasian Basin has a positive anomaly during 2009–2018 relative to its climatology (Fig. 11d), which may be related to more freshwater accumulated in the upper Amerasian Basin since mid-1990s (Fig. 8).

**2.5 Gateway transports**

In this subsection, the simulated ocean volume transport, heat transport, and liquid freshwater transport through the Bering
250  Strait, BSO, Fram Strait, and Davis Strait are evaluated. Ocean volume transport OVT, heat transport OHT, and freshwater transport FWT through each Arctic Ocean gateway are calculated as follows:

$$OVT = \int_{-H(\lambda)}^{0} \int_{\lambda_1(z)}^{\lambda_2(z)} v\, d\lambda dz, \tag{3}$$

$$OHT = \rho_o c_p \int_{-H(\lambda)}^{0} \int_{\lambda_1(z)}^{\lambda_2(z)} v(\theta - \theta_{ref})\, d\lambda dz, \tag{4}$$

$$FWT = \int_{-H(\lambda)}^{0} \int_{\lambda_1(z)}^{\lambda_2(z)} v(1 - S/S_{ref})\, d\lambda dz, \tag{5}$$

255  where v is ocean velocity normal to the section of each gateway, $\theta$ is the potential temperature, $\rho_o$ is seawater density, $c_p$ is the specific heat capacity of seawater, $\theta_{ref}$ is the reference temperature set to be 0 ℃, S is the salinity, $S_{ref}$ is the reference salinity set to be 34.8 psu, H is water depth, and $\lambda$ is the distance along the gateway transect.

### 2.5.1 Ocean volume transport

The mean net volume transport through the Bering Strait based on observations is 0.8±0.2 Sv (1 Sv ≡ $1 \times 10^6$ m$^3$/s) during
260  1990 to 2007 (Roach et al., 1995; Woodgate and Aagaard, 2005) and 1.0±0.05 Sv during 2003 to 2015 (Woodgate, 2018a).
The multi-model mean results of OMIP-1 and OMIP-2 in their last cycles are 1.0±0.1 and 1.1±0.1 Sv (Tables 2 and 3),
respectively. So, the climatology volume transport through the Bering Strait is reasonably simulated by both OMIP-1 and
OMIP-2. However, the observed positive trend in recent decades is not correctly reproduced in OMIP simulations.
Observations indicate that the volume transport has a positive trend (0.01 Sv/year) during 1990 to 2019 (Woodgate and
265  Peralta-Ferriz, 2021), while the trends in OMIP simulations are negative since 1990 (Figs. 12a, S11 and S12). The reasons
for the discrepancy between observations and simulations are unknown and should be further investigated. This seems to be
also an issue in models not part of OMIP and employing different atmospheric forcing (Nguyen et al., 2020).

The mean net volume transport through the BSO is ~2.0 Sv based on historical observations (Smedsrud et al., 2010, 2013).
The multi-model mean results of OMIP-1 and OMIP-2 in their last cycles are 3.0±0.5 and 3.3±0.4 Sv (Tables 2 and 3),
270  respectively. So this transport is overestimated in both OMIP-1 and OMIP-2 experiments (Fig. 12b). The trends of the net
volume transport in OMIP simulations over the simulated periods are not significant (Fig. 12b). There is no observation-
based estimation about the net volume trend, but Skagseth et al. (2020) estimated the volume flux of Atlantic Water inflow
to the Barents Sea based on an array of current meters in the western Barents Sea. They found that it increased by 0.2 Sv
over the period of 1998 to 2018 and the trend is not statistically significant.

275  The mean net volume transport through the Fram Strait is −2.0±2.7 Sv based on observations during 1997 to 2006 (Schauer
et al., 2008). The large uncertainty in the observations may be caused by the fact that the volumes of both inflow and outflow
through the Fram Strait are relatively large. The multi-model mean results of OMIP-1 and OMIP-2 are −2.3±0.5 and
−2.6±0.4 Sv (Tables 2 and 3), respectively. They are within the range of observational uncertainty.

The mean net volume transport through the Davis Strait is −1.6±0.5 Sv during 2004 to 2010 (Curry et al., 2014). The multi-
280  model mean results of OMIP-1 and OMIP-2 in their last cycles are −1.6±0.3 and −1.8±0.4 Sv (Tables 2 and 3), respectively.
So the multi-model mean results fit the observations well in both OMIP-1 and OMIP-2. OMIP2-2 simulated a decadal
increase in ocean volume export in the Davis Strait in the 2010s (Fig. 12d), which was induced by the dynamic sea level
drop south of Greenland in this period (Wang et al., 2022a).

Overall, the climatology of the net volume transports through the Arctic Ocean gateways is well represented in the multi-
285  model mean results of OMIP simulations. However, Tables 2 and 3 indicate that there are also large inter-model spreads in
OMIP models. The performance of CAS-ESM2-0 is quite different from other models (Table 2), for example, the net
volume transport through the Davis Strait in CAS-ESM2-0 is 0 Sv, and through the BSO is much smaller. The reason may
be that the passages in the Canadian Arctic Archipelago are closed in CAS-ESM2-0. Figures S11 and S12 indicate that
OMIP models are consistent in the inter-annual and decadal variability, and the variability in these two versions of the OMIP
290  simulations also agrees well.

### 2.5.2 Ocean heat transport

Ocean heat transport through the Bering Strait is ~9.5–19.0 TW computed using $\theta_{ref} = -1.9\,°C$ based on observations during 2001 to 2015 (Woodgate, 2018a). The multi-model mean results of OMIP-1 and OMIP-2 in their last cycles are 3.5±1.7 and 3.0±2.0 TW computed using $\theta_{ref} = 0\,°C$ (Tables 4 and 5), and 11.4±2.1 and 11.9±2.3 TW computed

295 using $\theta_{ref} = -1.9\,°C$, respectively. Thus the simulated mean ocean heat transport in OMIP fits the observations. A positive trend (0.35±0.17 TW/year) during 2000 to 2018 has been found based on observations (Woodgate and Peralta-Ferriz, 2021). The OMIP models obtained upward trends, but much weaker (0.13±0.26 TW/year in OMIP-2) (Fig. 12e). The weak trend is possibly caused by the erroneous negative trend in ocean volume transport in OMIP simulations shown in Fig. 12a.

Ocean heat transport through the BSO is the largest among the four gateways. Net ocean heat transport through the BSO is

300 48 and 74 TW based on the estimations by Skagseth et al. (2008) and Smedsrud et al. (2010), respectively. The multi-model mean results of OMIP-1 and OMIP-2 in their last cycles are 66.2±11.6 and 73.9±11.7 TW (Tables 4 and 5), respectively. Overall, OMIP multi-model mean results fit the observations. Its positive trend since 1980 reported by Skagseth et al. (2008), Årthun et al. (2012) and Wang et al. (2019a) can also be reproduced by both OMIP-1 and OMIP-2.

Based on the observational estimation by Schauer et al. (2008), ocean heat transport by Atlantic Water (warmer than 1 °C)

305 through the Fram Strait is between 26 and 50 TW without significant trend during 1997 to 2006. The multi-model mean net ocean heat transports of OMIP-1 and OMIP-2 in the last cycle are 21.2±3.7 and 20.6±6.0 TW (Tables 4 and 5), respectively. They are at the lower end of the observation-based estimate, which was also founded in CORE-II simulations (Ilicak et al., 2016). One possible reason may be that the observation-based estimate mentioned above is the heat transport in the Atlantic Water inflow but not the net ocean heat transport through the whole gateway. There is a clear increase in the heat transport in

310 the 2010s in OMIP-2, consistent with previous studies (Wang et al., 2020).

Ocean heat transport through the Davis Strait is 18±17 and 20±9 TW based on observations from 1987 to 1990 and from 2004 to 2005 (Cuny et al., 2005; Curry et al., 2011), respectively. The multi-model mean results of OMIP-1 and OMIP-2 in their last cycles are underestimated, being 12.6±2.4 and 13.8±3.1 TW (Tables 4 and 5), respectively.

Tables 4 and 5 show that OMIP models have large inter-model spreads in the simulations of the mean state of ocean heat

315 fluxes at all the four Arctic Ocean gateways. For the inter-annual and decadal variability, OMIP-1 and OMIP-2 models have relatively good agreement between their multi-model means (Fig. 12), although model spreads are also large for some of the heat fluxes (Figs. S11 and S12).

### 2.5.3 Freshwater transport

Ocean freshwater transport through the Bering Strait is $(2.4\pm0.3)\times10^3$ km3/year from 1990 to 2004 and $(2.3$–$3.5)\times10^3$

320 km$^3$/year between 2001 and 2015 based on observations (Woodgate and Aagaard, 2005; Woodgate, 2018a). Woodgate and Peralta-Ferriz (2021) also found that it has a significant positive trend [35±17 (km$^3$/year)/year] during 1990 to 2019 due to both the increase in ocean volume transport and the decrease in seawater salinity. The multi-model mean results of OMIP-1

and OMIP-2 in the last cycle are $(2.2 \pm 0.3) \times 10^3$ and $(2.4 \pm 0.3) \times 10^3$ (km³/year) (Tables 6 and 7), respectively. So OMIP models can reproduce the mean freshwater transport before 2004, but after that they significantly underestimate the

325 freshwater transport and show incorrect negative trends (Figs. 12i and S12i), mainly due to the negative trend in the simulated ocean volume transport (Figs. 12a and S12a).

Freshwater transport through the BSO is a freshwater sink for the Arctic Ocean with the annual mean value of $-0.09 \times 10^3$ km³/year based on historical observations (Serreze et al., 2006; Haine et al., 2015). The simulated freshwater transports are $(-0.58 \pm 0.22) \times 10^3$ and $(-0.48 \pm 0.18) \times 10^3$ km³/year in OMIP-1 and OMIP-2 (Tables 6 and 7), respectively. The

330 overestimation of the freshwater transport in the OMIP simulations may be caused by the overestimation of ocean volume transport (Fig. 12b).

Liquid freshwater transport through the Fram Strait is $-2.66 \pm 0.53$ km³/year based on historical observations (Serreze et al., 2006; Haine et al., 2015). It is also a freshwater sink of the Arctic Ocean. The multi-model mean results of OMIP-1 and OMIP-2 underestimated the observation, being $(-1.72 \pm 0.35) \times 10^3$ and $(-2.16 \pm 0.52) \times 10^3$ km³/year (Tables 6 and 7),

335 respectively. A strong increase in freshwater export at the beginning of the 2010s was simulated in OMIP-2 (Fig. 12k), consistent with the observed changes (de Steur et al., 2018).

Ocean freshwater transport through the Davis Strait is $(-2.93 \pm 0.19) \times 10^3$ km³/year based on historical observations during 2004 to 2010 (Curry et al., 2014). It is also a freshwater sink of the Arctic Ocean. The multi-model mean results of OMIP-1 and OMIP-2 in their last cycles are $(-2.54 \pm 0.46) \times 10^3$ and $(-3.27 \pm 0.62) \times 10^3$ km³/year (Tables 6 and 7), respectively. The

340 freshwater export in the Davis Strait increased in the 2010s in OMIP-2, owing to the increase in ocean volume export (Fig. 12d and l).

The freshwater transports in the multi-model means correlate well between OMIP-1 and OMIP-2 in their common simulation period. Similar to ocean volume and heat transports, ocean freshwater transport also has large inter-model spreads in OMIP simulations (Tables 6 and 7), but most OMIP models share similar inter-annual and decadal variability (Figs. S11

345 and S12). The freshwater flux through the Bering Strait has the best agreement among the models (Figs. S11 and S12), but its recent trend is incorrectly simulated in all the OMIP models (Figs. S11i and S12i).

## 3 Summary and Conclusions

In this work we assessed the Arctic Ocean simulations in 19 global ocean-sea ice models participating in CMIP6 OMIP (OMIP-1 and/or OMIP-2) (Griffies et al., 2016). The models used the same specified atmospheric forcing data sets and bulk

350 formula for surface flux calculations following the OMIP protocol. CORE2 forcing during 1948 to 2009 (Large and Yeager, 2009) and JRA55-do forcing during 1958 to 2018 (Tsujino et al., 2018) are the atmospheric forcing for OMIP-1 and OMIP-2 simulations, respectively. Modelled results of mean hydrography, liquid freshwater content, changes in Atlantic Water layer, upper ocean stratification, and gateway transports from the last cycle of the simulations were compared to the available observations and between the two OMIP versions.

355 Based on our evaluation, we concluded the following:

(1) For the simulations of the Arctic Ocean mean hydrography, most (but not all) models in OMIP can reproduce the vertical structures of temperature in the Arctic Ocean but with large biases and inter-model spreads, especially in the Atlantic Water layer depth range. The signal of warm Atlantic Water disappears too rapidly along the advection pathway in both OMIP-1 and OMIP-2 simulations compared to the observations. Most OMIP models suffer from too thick and deep Atlantic Water

360 layer and fresh biases in the halocline (50–400 m). OMIP model performances are similar to CORE-II in the representation of mean hydrography (Ilicak et al., 2016).

(2) For the simulations of the Arctic Ocean liquid freshwater content, OMIP-1 and OMIP-2 models show relatively good performance in simulating the inter-annual and decadal variability, being largely consistent with observations. However, they have large inter-model spreads in the simulation of the mean state. OMIP-2 has more liquid freshwater content than

365 OMIP-1. The overall performance of OMIP-1 and OMIP-2 in the simulation of freshwater content is also similar to CORE-II (Wang et al., 2016b).

(3) For temperature changes in the Atlantic Water layer, there is some disagreement between simulations and observations and between OMIP-1 and OMIP-2. The warming of Atlantic Water layer in the 1990s and especially in the 2000s in OMIP simulations is too weak compared to observations. The warming anomaly in the 2010s is captured in the OMIP-2

370 simulations. In addition, there are also clear effects of high temperature at the end of the preceding simulation cycles on the following cycle, which are more pronounced in OMIP-2.

(4) For the simulations of the Arctic Ocean stratification, the climatology of cold season surface mixed layer depth can be well reproduced by multi-model mean results of both OMIP-1 and OMIP-2, while the multi-model mean cold halocline base depths simulated by both OMIP-1 and OMIP-2 are much deeper than the PHC3.0 climatology, consistent with their fresh

375 biases in the halocline. OMIP models have large inter-model spreads in the simulation of the Arctic Ocean stratification.

(5) For the simulations of Arctic Ocean gateway transports, the climatology of the net volume transports through Arctic Ocean gateways is well reproduced by the multi-model mean results of OMIP simulations, although with large inter-model spreads. OMIP models are relatively good at representing the inter-annual and decadal variability of volume, heat and freshwater transports through the four Arctic Ocean gateways. OMIP models have the best agreement in the simulated

380 variability at the Bering Strait, but the recent upward trends in the Bering Strait fluxes are incorrectly simulated by both OMIP-1 and OMIP-2. Considering the important implications of Bering Strait inflow for the Arctic heat, freshwater and nutrients, this issue should be fixed to obtain more realistic Arctic Ocean simulations in global ocean-sea ice models. Relatively large biases are found in the climatological mean states of heat transport through the Fram Strait and freshwater transport through the BSO and Fram Strait.

385 (6) The OMIP models can better represent the interannual and decadal variability of Arctic Ocean gateway fluxes, freshwater content and upper ocean stratification than their mean states, similar to previous CORE-II models (Wang et al., 2016b)

Overall, no significant improvements were found in the Arctic Ocean simulations by global ocean-sea ice models from CORE-II to OMIP. The previously found large biases and inter-model spread in the Atlantic Water layer simulations remain

in OMIP-1 and OMIP-2. Therefore, it is not surprising that the large biases and inter-model spread are found in the Arctic
390  Ocean temperature and salinity simulations in CMIP6 fully-coupled models (Khosravi et al., 2022; Wang et al., 2022b).
Improving model parameterizations (e.g. horizontal and vertical mixing) and using higher model resolutions may be possible
solutions. The horizontal resolutions in OMIP models are mostly coarse (nominal 1°, 24–50 km in the Arctic) (Table 1).
Wang et al. (2018) shows that a model with 4.5-km resolution in the Arctic Ocean performs much better than a 24-km
resolution model, especially in the simulations of the Atlantic Water layer, indicating that higher resolution (eddy permitting
395  to eddy resolving) can help reduce model biases in the Arctic Ocean simulations. In addition, simulations with different
resolutions need to be evaluated in a more careful and comprehensive way under a common multi-model framework in the
future.

We did not find significant improvement in simulating Arctic Ocean using JRA55-do forcing than using CORE2 forcing.
However, the simulated variability and trends of freshwater content and gateways transports agree well between OMIP-1 and
400  OMIP-2. Therefore, JRA55-do forcing which has been updated to date is a good alternative to CORE2 forcing for studying
recent changes in the Arctic Ocean. Part of the difference in the simulated temperature, salinity, and cold halocline base
depth between OMIP-1 and OMIP-2 is caused by the design of the OMIP simulations. Repeating the full cycle of the
atmosphere forcing can leave a large amount of Arctic Ocean heat and freshwater from the preceding simulation cycle to the
following cycle. Our analysis suggests to only repeat the atmosphere forcing in the 20th century which has relatively weak
405  climate change signal in the model spinup cycles.

**Code availability**

Matlab code used to process data and generate figures is available at https://zenodo.org/record/7250913#.Y1iDDfmhW6s.

**Data availability**

OMIP-1 and OMIP-2 datasets are available at https://esgf-node.llnl.gov/search/cmip6/.

410  **Author contribution**

QS, QW and CG proposed and led this evaluation study. QS, SW and YH processed the model outputs and produced the
figures. All authors contributed to the writing and editing processes.

**Competing interests**

The authors declare that they have no conflict of interest.

## Acknowledgments

Qi Shu was supported by the Chinese Natural Science Foundation (41941012) and the Taishan Scholars Program. Qiang Wang was supported by the Helmholtz Climate Initiative REKLIM (Regional Climate Change and Human) and the EPICA project in the research theme "MARE:N – Polarforschung/MOSAiC" funded by the German Federal Ministry for Education and Research with funding number 03F0889A. Chuncheng Guo acknowledges support from the Research Council of Norway funded projects KeyPOCP (328941) and KeyClim (295046). This work is a contribution to the UN Decade of Ocean Science for Sustainable Development (2021-2030) through both the Decade Collaborative Centre on Ocean-Climate nexus and Coordination amongst decade implementing partners in P. R. China (DCC-OCC) and the approved Programme of the Ocean to climate Seamless Forecasting system (OSF). OMIP-1 and OMIP-2 data are from https://esgf-node.llnl.gov/search/cmip6/. The PHC3.0 climatology dataset was downloaded from http://psc.apl.washington.edu/nonwp_projects/PHC/Climatology.html. We would like to thank the above data providers.

## References

Aagaard, K. and Carmack, E. C.: The role of sea ice and other fresh water in the Arctic circulation, J. Geophys. Res., 94, 14485, https://doi.org/10.1029/jc094ic10p14485, 1989.

Aksenov, Y., Karcher, M., Proshutinsky, A., Gerdes, R., de Cuevas, B., Golubeva, E., Kauker, F., Nguyen, A. T., Platov, G. A., Wadley, M., Watanabe, E., Coward, A. C., and Nurser, A. J. G.: Arctic pathways of Pacific Water: Arctic Ocean Model Intercomparison experiments, J. Geophys. Res. Ocean., 121, 27–59, https://doi.org/10.1002/2015JC011299, 2016.

Årthun, M., Eldevik, T., Smedsrud, L. H., Skagseth, and Ingvaldsen, R. B.: Quantifying the influence of atlantic heat on barents sea ice variability and retreat, J. Clim., 25, 4736–4743, https://doi.org/10.1175/JCLI-D-11-00466.1, 2012.

Beszczynska-Möller, A., Fahrbach, E., Schauer, U., and Hansen, E.: Variability in Atlantic water temperature and transport at the entrance to the Arctic Ocean, 1997–2010, ICES J. Mar. Sci., 69, 852–863, https://doi.org/10.1093/icesjms/fss056, 2012.

Bourgain, P. and Gascard, J. C.: The arctic ocean halocline and its interannual variability from 1997 to 2008, Deep. Res. Part I Oceanogr. Res. Pap., 58, 745–756, https://doi.org/10.1016/j.dsr.2011.05.001, 2011.

Cohen, J., Zhang, X., Francis, J., Jung, T., Kwok, R., Overland, J., Ballinger, T. J., Bhatt, U. S., Chen, H. W., Coumou, D., Feldstein, S., Gu, H., Handorf, D., Henderson, G., Ionita, M., Kretschmer, M., Laliberte, F., Lee, S., Linderholm, H. W., Maslowski, W., Peings, Y., Pfeiffer, K., Rigor, I., Semmler, T., Stroeve, J., Taylor, P. C., Vavrus, S., Vihma, T., Wang, S., Wendisch, M., Wu, Y., and Yoon, J.: Divergent consensuses on Arctic amplification influence on midlatitude severe winter weather, 20–29 pp., https://doi.org/10.1038/s41558-019-0662-y, 2020.

Cuny, J., Rhines, P. B., and Kwok, R.: Davis Strait volume, freshwater and heat fluxes, Deep. Res. Part I Oceanogr. Res. Pap., 52, 519–542, https://doi.org/10.1016/j.dsr.2004.10.006, 2005.

Curry, B., Lee, C. M., and Petrie, B.: Volume, freshwater, and heat fluxes through Davis Strait, 2004-05, J. Phys. Oceanogr., 41, 429–436, https://doi.org/10.1175/2010JPO4536.1, 2011.

Curry, B., Lee, C. M., Petrie, B., Moritz, R. E., and Kwok, R.: Multiyear volume, liquid freshwater, and sea ice transports through Davis Strait, 2004-10, J. Phys. Oceanogr., 44, 1244–1266, https://doi.org/10.1175/JPO-D-13-0177.1, 2014.

450 Dai, A. and Trenberth, K. E.: Estimates of Freshwater Discharge from Continents: Latitudinal and Seasonal Variations, J. Hydrometeorol., 3, 660–687, https://doi.org/10.1175/1525-7541(2002)003<0660:EOFDFC>2.0.CO;2, 2002.

Dai, A., Qian, T., Trenberth, K. E., and Milliman, J. D.: Changes in continental freshwater discharge from 1948 to 2004, J. Clim., 22, 2773–2792, https://doi.org/10.1175/2008JCLI2592.1, 2009.

Danielson, S. L., Ahkinga, O., Ashjian, C., Basyuk, E., Cooper, L. W., Eisner, L., Farley, E., Iken, K. B., Grebmeier, J. M.,
455 Juranek, L., Khen, G., Jayne, S. R., Kikuchi, T., Ladd, C., Lu, K., McCabe, R. M., Moore, G. W. K., Nishino, S., Ozenna, F., Pickart, R. S., Polyakov, I., Stabeno, P. J., Thoman, R., Williams, W. J., Wood, K., and Weingartner, T. J.: Manifestation and consequences of warming and altered heat fluxes over the Bering and Chukchi Sea continental shelves, Deep. Res. Part II Top. Stud. Oceanogr., 177, https://doi.org/10.1016/j.dsr2.2020.104781, 2020.

Dickson, R., Rudels, B., Dye, S., Karcher, M., Meincke, J., and Yashayaev, I.: Current estimates of freshwater flux through
460 Arctic and subarctic seas, Prog. Oceanogr., 73, 210–230, https://doi.org/10.1016/j.pocean.2006.12.003, 2007.

Golubeva, E. N. and Platov, G. A.: On improving the simulation of Atlantic Water circulation in the Arctic Ocean, J. Geophys. Res. Ocean., 112, 1–16, https://doi.org/10.1029/2006JC003734, 2007.

Goosse, H., Fichefet, T., and Campin, J. M.: The effects of the water flow through the Canadian Archipelago in a global ice-ocean model, Geophys. Res. Lett., 24, 1507–1510, https://doi.org/10.1029/97GL01352, 1997.

465 Griffies, S. M., Biastoch, A., Böning, C., Bryan, F., Danabasoglu, G., Chassignet, E. P., England, M. H., Gerdes, R., Haak, H., Hallberg, R. W., Hazeleger, W., Jungclaus, J., Large, W. G., Madec, G., Pirani, A., Samuels, B. L., Scheinert, M., Gupta, A. Sen, Severijns, C. A., Simmons, H. L., Treguier, A. M., Winton, M., Yeager, S., and Yin, J.: Coordinated Ocean-ice Reference Experiments (COREs), Ocean Model., 26, 1–46, https://doi.org/10.1016/j.ocemod.2008.08.007, 2009.

Griffies, S. M., Winton, M., Samuels, B., Danabasoglu, G., Yeager, S. G., Marlsand, S., Drange, H., and Bentsen, M.:
470 Datasets and protocol for the CLIVAR WGOMD Coordinated Ocean-sea ice Reference Experiments ( COREs ), ICPO Publ. Ser., 21, 2012.

Griffies, S. M., Danabasoglu, G., Durack, P. J., Adcroft, A. J., Balaji, V., Boning, C. W., Chassignet, E. P., Curchitser, E., Deshayes, J., and Drange, H.: OMIP contribution to CMIP6: experimental and diagnostic protocol for the physical component of the Ocean Model Intercomparison Project, Geosci. Model Dev., 3231–3296, 2016.

475 Haine, T. W. N., Curry, B., Gerdes, R., Hansen, E., Karcher, M., Lee, C., Rudels, B., Spreen, G., de Steur, L., Stewart, K. D., and Woodgate, R.: Arctic freshwater export: Status, mechanisms, and prospects, Glob. Planet. Change, 125, 13–35, https://doi.org/10.1016/j.gloplacha.2014.11.013, 2015.

Holloway, G., Dupont, F., Golubeva, E., Häkkinen, S., Hunke, E., Jin, M., Karcher, M., Kauker, F., Maltrud, M., Morales Maqueda, M. A., Maslowski, W., Platov, G., Stark, D., Steele, M., Suzuki, T., Wang, J., and Zhang, J.: Water properties and circulation in Arctic Ocean models, J. Geophys. Res. Ocean., 112, 1–18, https://doi.org/10.1029/2006JC003642, 2007.

Hu, X., Myers, P. G., and Lu, Y.: Pacific Water Pathway in the Arctic Ocean and Beaufort Gyre in Two Simulations With Different Horizontal Resolutions, J. Geophys. Res. Ocean., 124, 6414–6432, https://doi.org/10.1029/2019JC015111, 2019.

Ilicak, M., Drange, H., Wang, Q., Gerdes, R., Aksenov, Y., Bailey, D., Bentsen, M., Biastoch, A., Bozec, A., Böning, C., Cassou, C., Chassignet, E., Coward, A. C., Curry, B., Danabasoglu, G., Danilov, S., Fernandez, E., Fogli, P. G., Fujii, Y., Griffies, S. M., Iovino, D., Jahn, A., Jung, T., Large, W. G., Lee, C., Lique, C., Lu, J., Masina, S., George Nurser, A. J., Roth, C., Salas y Mélia, D., Samuels, B. L., Spence, P., Tsujino, H., Valcke, S., Voldoire, A., Wang, X., and Yeager, S. G.: An assessment of the Arctic Ocean in a suite of interannual CORE-II simulations. Part III: Hydrography and fluxes, Ocean Model., 100, 141–161, https://doi.org/10.1016/j.ocemod.2016.02.004, 2016.

Ingvaldsen, R. B., Assmann, K. M., Primicerio, R., Fossheim, M., Polyakov, I. V., and Dolgov, A. V.: Physical manifestations and ecological implications of Arctic Atlantification, Nat. Rev. Earth Environ., 2, 874–889, https://doi.org/10.1038/s43017-021-00228-x, 2021.

Jahn, A., Aksenov, Y., De Cuevas, B. A., De Steur, L., Häkkinen, S., Hansen, E., Herbaut, C., Houssais, M. N., Karcher, M., Kauker, F., Lique, C., Nguyen, A., Pemberton, P., Worthen, D., and Zhang, J.: Arctic Ocean freshwater: How robust are model simulations?, J. Geophys. Res. Ocean., 117, https://doi.org/10.1029/2012JC007907, 2012.

Jungclaus, J. H., Haak, H., Latif, M., and Mikolajewicz, U.: Arctic–North Atlantic Interactions and Multidecadal Variability of the Meridional Overturning Circulation, J. Clim., 18, 4013–4031, https://doi.org/10.1175/JCLI3462.1, 2005.

Karcher, M. J.: Pathways and modification of the upper and intermediate waters of the Arctic Ocean, J. Geophys. Res., 107, 1–13, https://doi.org/10.1029/2000jc000530, 2002.

Karcher, M. J., Gerdes, R., Kauker, F., and Köberle, C.: Arctic warming: Evolution and spreading of the 1990s warm event in the Nordic seas and the Arctic Ocean, J. Geophys. Res. Ocean., 108, https://doi.org/10.1029/2001jc001265, 2003.

Khosravi, N., Wang, Q., Koldunov, N., Hinrichs, C., Semmler, T., Danilov, S., and Jung, T.: The Arctic Ocean in CMIP6 Models: Biases and Projected Changes in Temperature and Salinity, Earth's Futur., 10, https://doi.org/10.1029/2021ef002282, 2022.

Kim, B. M., Son, S. W., Min, S. K., Jeong, J. H., Kim, S. J., Zhang, X., Shim, T., and Yoon, J. H.: Weakening of the stratospheric polar vortex by Arctic sea-ice loss, Nat. Commun., 5, https://doi.org/10.1038/ncomms5646, 2014.

Kobayashi, S., Ota, Y., Harada, Y., Ebita, A., Moriya, M., Onoda, H., Onogi, K., Kamahori, H., Kobayashi, C., and Endo, H.: The JRA-55 reanalysis: General specifications and basic characteristics, J. Meteorol. Soc. Japan. Ser. II, 93, 5–48, 2015.

Large, W. G. and Yeager, S. G.: The global climatology of an interannually varying air - Sea flux data set, Clim. Dyn., 33, 341–364, https://doi.org/10.1007/s00382-008-0441-3, 2009.

Li, F., Wan, X., Wang, H., Orsolini, Y. J., Cong, Z., Gao, Y., and Kang, S.: Arctic sea-ice loss intensifies aerosol transport to the Tibetan Plateau, Nat. Clim. Chang., 10, 1037–1044, https://doi.org/10.1038/s41558-020-0881-2, 2020.

Li, Z., Ding, Q., Steele, M., and Schweiger, A.: Recent upper Arctic Ocean warming expedited by summertime atmospheric processes, Nat. Commun., 13, 1–11, https://doi.org/10.1038/s41467-022-28047-8, 2022.

Lique, C., Treguier, A. M., Blanke, B., and Grima, N.: On the origins of water masses exported along both sides of

515 Greenland: A Lagrangian model analysis, J. Geophys. Res. Ocean., 115, 1–20, https://doi.org/10.1029/2009JC005316, 2010.

Locarnini, R. A., Mishonov, A. V, Antonov, J. I., Boyer, T. P., Garcia, H. E., Baranova, O. K., Zweng, M. M., Paver, C. R., Reagan, J. R., and Johnson, D. R.: World ocean atlas 2013. Volume 1, Temperature, 2013.

Maslowski, W., Marble, D., Walczowski, W., Schauer, U., Clement, J. L., and Semtner, A. J.: On climatological mass, heat, and salt transports through the Barents Sea and Fram strait from a pan-Arctic coupled ice-ocean model simulation, J.

520 Geophys. Res. Ocean., 109, 1–16, https://doi.org/10.1029/2001jc001039, 2004.

Na, L., Jiping, L., Zhanhai, Z., Hongxia, C., and Mirong, S.: Is extreme Arctic sea ice anomaly in 2007 a key contributor to severe January 2008 snowstorm in China?, Int. J. Climatol., 32, 2081–2087, https://doi.org/10.1002/joc.2400, 2012.

Nguyen, A. T., Menemenlis, D., and Kwok, R.: Improved modeling of the arctic halocline with a subgrid-scale brine rejection parameterization, J. Geophys. Res. Ocean., 114, 1–12, https://doi.org/10.1029/2008JC005121, 2009.

525 Nguyen, A. T., Woodgate, R. A., and Heimbach, P.: Elucidating Large-Scale Atmospheric Controls on Bering Strait Throughflow Variability Using a Data-Constrained Ocean Model and Its Adjoint, J. Geophys. Res. Ocean., 125, https://doi.org/10.1029/2020JC016213, 2020.

Onarheim, I. H., Eldevik, T., Smedsrud, L. H., and Stroeve, J. C.: Seasonal and regional manifestation of Arctic sea ice loss, J. Clim., 31, 4917–4932, https://doi.org/10.1175/JCLI-D-17-0427.1, 2018.

530 Outten, S. D. and Esau, I.: A link between Arctic sea ice and recent cooling trends over Eurasia, Clim. Change, 110, 1069–1075, https://doi.org/10.1007/s10584-011-0334-z, 2012.

Peralta-Ferriz, C. and Woodgate, R. A.: Seasonal and interannual variability of pan-Arctic surface mixed layer properties from 1979 to 2012 from hydrographic data, and the dominance of stratification for multiyear mixed layer depth shoaling, Prog. Oceanogr., 134, 19–53, https://doi.org/10.1016/j.pocean.2014.12.005, 2015.

535 Polyakov, I. V., Alekseev, G. V., Timokhov, L. A., Bhatt, U. S., Colony, R. L., Simmons, H. L., Walsh, D., Walsh, J. E., and Zakharov, V. F.: Variability of the intermediate Atlantic water of the Arctic Ocean over the last 100 years, J. Clim., 17, 4485–4497, https://doi.org/10.1175/JCLI-3224.1, 2004.

Polyakov, I. V., Pnyushkov, A. V., and Timokhov, L. A.: Warming of the intermediate Atlantic water of the Arctic ocean in the 2000S, J. Clim., 25, 8362–8370, https://doi.org/10.1175/JCLI-D-12-00266.1, 2012.

540 Polyakov, I. V., Bhatt, U. S., Walsh, J. E., Abrahamsen, E. P., Pnyushkov, A. V., and Wassmann, P. F.: Recent oceanic changes in the Arctic in the context of long-term observations, Ecol. Appl., 23, 1745–1764, https://doi.org/10.1890/11-0902.1, 2013.

Polyakov, I. V., Pnyushkov, A. V., Alkire, M. B., Ashik, I. M., Baumann, T. M., Carmack, E. C., Goszczko, I., Guthrie, J., Ivanov, V. V., Kanzow, T., Krishfield, R., Kwok, R., Sundfjord, A., Morison, J., Rember, R., and Yulin, A.: Greater role for

545    Atlantic inflows on sea-ice loss in the Eurasian Basin of the Arctic Ocean, Science (80-. )., 356, 285–291,
       https://doi.org/10.1126/science.aai8204, 2017.

Polyakov, I. V., Alkire, M. B., Bluhm, B. A., Brown, K. A., Carmack, E. C., Chierici, M., Danielson, S. L., Ellingsen, I.,
Ershova, E. A., Gårdfeldt, K., Ingvaldsen, R. B., Pnyushkov, A. V., Slagstad, D., and Wassmann, P.: Borealization of the
Arctic Ocean in Response to Anomalous Advection From Sub-Arctic Seas, Front. Mar. Sci., 7, 7–8,

550    https://doi.org/10.3389/fmars.2020.00491, 2020a.

Polyakov, I. V., Alkire, M. B., Bluhm, B. A., Brown, K. A., Carmack, E. C., Chierici, M., Danielson, S. L., Ellingsen, I.,
Ershova, E. A., Gårdfeldt, K., Ingvaldsen, R. B., Pnyushkov, A. V., Slagstad, D., and Wassmann, P.: Borealization of the
Arctic Ocean in Response to Anomalous Advection From Sub-Arctic Seas, Front. Mar. Sci., 7,
       https://doi.org/10.3389/fmars.2020.00491, 2020b.

555    Polyakov, I. V., Rippeth, T. P., Fer, I., Alkire, M. B., Baumann, T. M., Carmack, E. C., Ingvaldsen, R., Ivanov, V. V., Janout,
M., Lind, S., Padman, L., Pnyushkov, A. V., and Rember, R.: Weakening of cold halocline layer exposes sea ice to oceanic
heat in the eastern arctic ocean, J. Clim., 33, 8107–8123, https://doi.org/10.1175/JCLI-D-19-0976.1, 2020c.

Proshutinsky, A., Steele, M., Zhang, J., Holloway, G., Steiner, N., Hakkinen, S., Holland, D., Gerdes, R., Koeberle, C.,
Karcher, M., Johnson, M., Maslowski, W., Walczowski, W., Hibler, W., and Wang, J.: Multinational effort studies

560    differences among Arctic Ocean models, Eos, Trans. Am. Geophys. Union, 82, 637–637, https://doi.org/10.1029/01eo00365,
       2001.

Proshutinsky, A., Bourke, R. H., and McLaughlin, F. A.: The role of the Beaufort Gyre in Arctic climate variability:
Seasonal to decadal climate scales, Geophys. Res. Lett., 29, 1–4, https://doi.org/10.1029/2002GL015847, 2002.

Proshutinsky, A., Ashik, I., Häkkinen, S., Hunke, E., Krishfield, R., Maltrud, M., Maslowski, W., and Zhang, J.: Sea level

565    variability in the Arctic Ocean from AOMIP models, J. Geophys. Res. Ocean., 112, 1–25,
       https://doi.org/10.1029/2006JC003916, 2007.

Proshutinsky, A., Krishfield, R., Timmermans, M.-L., Toole, J., Carmack, E., McLaughlin, F., Williams, W. J.,
Zimmermann, S., Itoh, M., and Shimada, K.: Beaufort Gyre freshwater reservoir: State and variability from observations, J.
Geophys. Res., 114, 1–25, https://doi.org/10.1029/2008jc005104, 2009.

570    Proshutinsky, A., Steele, M., and Timmermans, M.-L.: Forum for Arctic Modeling and Observational Synthesis (FAMOS):
Past, current, and future activities, J. Geophys. Res. Ocean., 121, 3803–3819, https://doi.org/10.1002/2016JC011898, 2016.

Proshutinsky, A., Krishfield, R., Toole, J. M., Timmermans, M. L., Williams, W., Zimmermann, S., Yamamoto-Kawai, M.,
Armitage, T. W. K., Dukhovskoy, D., Golubeva, E., Manucharyan, G. E., Platov, G., Watanabe, E., Kikuchi, T., Nishino, S.,
Itoh, M., Kang, S. H., Cho, K. H., Tateyama, K., and Zhao, J.: Analysis of the Beaufort Gyre Freshwater Content in 2003–

575    2018, J. Geophys. Res. Ocean., 124, 9658–9689, https://doi.org/10.1029/2019JC015281, 2019.

Rabe, B., Karcher, M., Kauker, F., Schauer, U., Toole, J. M., Krishfield, R. A., Pisarev, S., Kikuchi, T., and Su, J.: Arctic
Ocean basin liquid freshwater storage trend 1992-2012, Geophys. Res. Lett., 41, 961–968,
https://doi.org/10.1002/2013GL058121, 2014.

Roach, A. T., Aagaard, K., Pease, C. H., Salo, S. A., Weingartner, T., Pavlov, V., and Kulakov, M.: Direct measurements of
580    transport and water properties through the Bering Strait, J. Geophys. Res., 100, 18443, https://doi.org/10.1029/95JC01673,
1995.

Rudels, B.: Arctic Ocean Circulation, Encycl. Ocean Sci., 211–225, https://doi.org/10.1016/B978-012374473-9.00601-9,
2009.

Rudels, B., Korhonen, M., Schauer, U., Pisarev, S., Rabe, B., and Wisotzki, A.: Circulation and transformation of Atlantic
585    water in the Eurasian Basin and the contribution of the Fram Strait inflow branch to the Arctic Ocean heat budget, Prog.
Oceanogr., 132, 128–152, https://doi.org/10.1016/j.pocean.2014.04.003, 2015.

Schauer, U., Loeng, H., Rudels, B., Ozhigin, V. K., and Dieck, W.: Atlantic Water flow through the Barents and Kara Seas,
Deep. Res. Part I Oceanogr. Res. Pap., 49, 2281–2298, https://doi.org/10.1016/S0967-0637(02)00125-5, 2002.

Schauer, U., Beszczynska-Möller, A., Walczowski, W., Fahrbach, E., Piechura, J., and Hansen, E.: Variation of Measured
590    Heat Flow Through the Fram Strait Between 1997 and 2006 BT - Arctic Subarctic Ocean Fluxes: Defining the Role of the
Northern Seas in Climate, Arctic–Subarctic Ocean Fluxes, 65–85, 2008.

Serreze, M. C., Barrett, A. P., Slater, A. G., Woodgate, R. A., Aagaard, K., Lammers, R. B., Steele, M., Moritz, R., Meredith,
M., and Lee, C. M.: The large-scale freshwater cycle of the Arctic, J. Geophys. Res. Ocean., 111, 1–19,
https://doi.org/10.1029/2005JC003424, 2006.

595    Shu, Q., Qiao, F., Song, Z., and Xiao, B.: Effect of increasing Arctic river runoff on the Atlantic meridional overturning
circulation: a model study, Acta Oceanol. Sin., 36, 59–65, https://doi.org/10.1007/s13131-017-1009-z, 2017.

Shu, Q., Wang, Q., Su, J., Li, X., and Qiao, F.: Assessment of the Atlantic water layer in the Arctic Ocean in CMIP5 climate
models, Clim. Dyn., 53, 5279–5291, https://doi.org/10.1007/s00382-019-04870-6, 2019.

Shu, Q., Wang, Q., Årthun, M., Wang, S., and Song, Z.: Arctic Ocean Amplification in a warming climate in CMIP6 models,
600    1–11, 2022.

Skagseth, Ø., Furevik, T., Ingvaldsen, R., Loeng, H., Mork, K. A., Orvik, K. A., and Ozhigin, V.: Volume and Heat
Transports to the Arctic Ocean Via the Norwegian and Barents Seas, in: Arctic–Subarctic Ocean Fluxes, edited by: Dickson,
R. R., Meincke, J., and Rhines, P., Springer Netherlands, Dordrecht, 45–64, https://doi.org/10.1007/978-1-4020-6774-7_3,
2008.

605    Skagseth, Ø., Eldevik, T., Årthun, M., Asbjørnsen, H., Lien, V. S., and Smedsrud, L. H.: Reduced efficiency of the Barents
Sea cooling machine, Nat. Clim. Chang., 10, 661–666, https://doi.org/10.1038/s41558-020-0772-6, 2020.

Smedsrud, L. H., Ingvaldsen, R., Nilsen, J. E. Ø., and Skagseth: Heat in the Barents Sea: Transport, storage, and surface
fluxes, Ocean Sci., 6, 219–234, https://doi.org/10.5194/os-6-219-2010, 2010.

Smedsrud, L. H., Esau, I., Ingvaldsen, R. B., Eldevik, T., Haugan, P. M., Li, C., Lien, V. S., Olsen, A., Omar, A. M.,
610    Risebrobakken, B., Sandø, A. B., Semenov, V. A., and Sorokina, S. A.: The role of the Barents Sea in the Arctic climate
system, Rev. Geophys., 51, 415–449, https://doi.org/10.1002/rog.20017, 2013.

Solomon, A., Heuzé, C., Rabe, B., Bacon, S., Bertino, L., Heimbach, P., Inoue, J., Iovino, D., Mottram, R., Zhang, X., Aksenov, Y., McAdam, R., Nguyen, A., Raj, R. P., and Tang, H.: Freshwater in the Arctic Ocean 2010-2019, Ocean Sci., 17, 1081–1102, https://doi.org/10.5194/os-17-1081-2021, 2021.

615    Steele, M. and Boyd, T.: Retreat of the cold halocline layer in the Arctic Ocean, J. Geophys. Res. Ocean., 103, 10419–10435, https://doi.org/10.1029/98JC00580, 1998.

Steele, M., Morley, R., and Ermold, W.: PHC: A global ocean hydrography with a high-quality Arctic Ocean, J. Clim., 14, 2079–2087, https://doi.org/10.1175/1520-0442(2001)014<2079:PAGOHW>2.0.CO;2, 2001.

Steele, M., Morison, J., Ermold, W., Rigor, I., Ortmeyer, M., and Shimada, K.: Circulation of summer Pacific halocline

620    water in the Arctic Ocean, J. Geophys. Res. Ocean., 109, 1–18, https://doi.org/10.1029/2003jc002009, 2004.

Steele, M., Ermold, W., and Zhang, J.: Arctic Ocean surface warming trends over the past 100 years, Geophys. Res. Lett., 35, 1–6, https://doi.org/10.1029/2007GL031651, 2008.

de Steur, L., Peralta-Ferriz, C., and Pavlova, O.: Freshwater Export in the East Greenland Current Freshens the North Atlantic, Geophys. Res. Lett., 45, 13,359-13,366, https://doi.org/10.1029/2018GL080207, 2018.

625    Stroeve, J. and Notz, D.: Changing state of Arctic sea ice across all seasons, Environ. Res. Lett., 13, https://doi.org/10.1088/1748-9326/aade56, 2018.

Timmermans, M. L. and Marshall, J.: Understanding Arctic Ocean Circulation: A Review of Ocean Dynamics in a Changing Climate, J. Geophys. Res. Ocean., 125, 1–35, https://doi.org/10.1029/2018JC014378, 2020.

Tsujino, H., Urakawa, S., Nakano, H., Small, R. J., Kim, W. M., Yeager, S. G., Danabasoglu, G., Suzuki, T., Bamber, J. L.,

630    and Bentsen, M.: JRA-55 based surface dataset for driving ocean–sea-ice models (JRA55-do), Ocean Model., 130, 79–139, 2018.

Tsujino, H., Urakawa, L. S., Griffies, S. M., Danabasoglu, G., Adcroft, A. J., Amaral, A. E., Arsouze, T., Bentsen, M., Bernardello, R., Böning, C. W., Bozec, A., Chassignet, E. P., Danilov, S., Dussin, R., Exarchou, E., Fogli, P. G., Fox-Kemper, B., Guo, C., Ilicak, M., Iovino, D., Kim, W. M., Koldunov, N., Lapin, V., Li, Y., Lin, P., Lindsay, K., Liu, H., Long,

635    M. C., Komuro, Y., Marsland, S. J., Masina, S., Nummelin, A., Rieck, J. K., Ruprich-Robert, Y., Scheinert, M., Sicardi, V., Sidorenko, D., Suzuki, T., Tatebe, H., Wang, Q., Yeager, S. G., and Yu, Z.: Evaluation of global ocean–sea-ice model simulations based on the experimental protocols of the Ocean Model Intercomparison Project phase 2 (OMIP-2), 3643–3708 pp., https://doi.org/10.5194/gmd-13-3643-2020, 2020.

Våge, K., Pickart, R. S., Pavlov, V., Lin, P., Torres, D. J., Ingvaldsen, R., Sundfjord, A., and Proshutinsky, A.: The Atlantic

640    Water boundary current in the Nansen Basin: Transport and mechanisms of lateral exchange, J. Geophys. Res. Ocean., 121, 6946–6960, https://doi.org/10.1002/2016JC011715, 2016.

Wadley, M. R. and Bigg, G. R.: Impact of flow through the Canadian Archipelago and Bering Strait on the North Atlantic and Arctic circulation: An ocean modelling study, Q. J. R. Meteorol. Soc., 128, 2187–2203, https://doi.org/10.1256/qj.00.35, 2002.

645 Wang, Q. and Danilov, S.: A Synthesis of the Upper Arctic Ocean Circulation During 2000–2019: Understanding the Roles of Wind Forcing and Sea Ice Decline, Front. Mar. Sci., 9, 1–24, https://doi.org/10.3389/fmars.2022.863204, 2022.

Wang, Q., Ilicak, M., Gerdes, R., Drange, H., Aksenov, Y., Bailey, D. A., Bentsen, M., Biastoch, A., Bozec, A., Böning, C., Cassou, C., Chassignet, E., Coward, A. C., Curry, B., Danabasoglu, G., Danilov, S., Fernandez, E., Fogli, P. G., Fujii, Y., Griffies, S. M., Iovino, D., Jahn, A., Jung, T., Large, W. G., Lee, C., Lique, C., Lu, J., Masina, S., Nurser, A. J. G., Rabe, B.,
650 Roth, C., Salas y Mélia, D., Samuels, B. L., Spence, P., Tsujino, H., Valcke, S., Voldoire, A., Wang, X., and Yeager, S. G.: An assessment of the Arctic Ocean in a suite of interannual CORE-II simulations. Part I: Sea ice and solid freshwater, Ocean Model., 99, 110–132, https://doi.org/10.1016/j.ocemod.2015.12.008, 2016a.

Wang, Q., Ilicak, M., Gerdes, R., Drange, H., Aksenov, Y., Bailey, D. A., Bentsen, M., Biastoch, A., Bozec, A., Böning, C., Cassou, C., Chassignet, E., Coward, A. C., Curry, B., Danabasoglu, G., Danilov, S., Fernandez, E., Fogli, P. G., Fujii, Y.,
655 Griffies, S. M., Iovino, D., Jahn, A., Jung, T., Large, W. G., Lee, C., Lique, C., Lu, J., Masina, S., Nurser, A. J. G., Rabe, B., Roth, C., Salas y Mélia, D., Samuels, B. L., Spence, P., Tsujino, H., Valcke, S., Voldoire, A., Wang, X., and Yeager, S. G.: An assessment of the Arctic Ocean in a suite of interannual CORE-II simulations. Part II: Liquid freshwater, Ocean Model., 99, 86–109, https://doi.org/10.1016/j.ocemod.2015.12.009, 2016b.

Wang, Q., Wekerle, C., Danilov, S., Wang, X., and Jung, T.: A 4.5g km resolution Arctic Ocean simulation with the global
660 multi-resolution model FESOM 1.4, Geosci. Model Dev., 11, 1229–1255, https://doi.org/10.5194/gmd-11-1229-2018, 2018.

Wang, Q., Wang, X., Wekerle, C., Danilov, S., Jung, T., Koldunov, N., Lind, S., Sein, D., Shu, Q., and Sidorenko, D.: Ocean Heat Transport Into the Barents Sea: Distinct Controls on the Upward Trend and Interannual Variability, Geophys. Res. Lett., 46, 13180–13190, https://doi.org/10.1029/2019GL083837, 2019a.

Wang, Q., Wekerle, C., Danilov, S., Sidorenko, D., Koldunov, N., Sein, D., Rabe, B., and Jung, T.: Recent sea ice decline
665 did not significantly increase the total liquid freshwater content of the Arctic Ocean, J. Clim., 32, 15–32, https://doi.org/10.1175/JCLI-D-18-0237.1, 2019b.

Wang, Q., Wekerle, C., Wang, X., Danilov, S., Koldunov, N., Sein, D., Sidorenko, D., von Appen, W. J., and Jung, T.: Intensification of the Atlantic Water Supply to the Arctic Ocean Through Fram Strait Induced by Arctic Sea Ice Decline, Geophys. Res. Lett., 47, https://doi.org/10.1029/2019GL086682, 2020.

670 Wang, Q., Danilov, S., Sidorenko, D., and Wang, X.: Circulation Pathways and Exports of Arctic River Runoff Influenced by Atmospheric Circulation Regimes, Front. Mar. Sci., 8, 1–23, https://doi.org/10.3389/fmars.2021.707593, 2021.

Wang, Q., Shu, Q., Danilov, S., and Sidorenko, D.: An extreme event of enhanced Arctic Ocean export west of Greenland caused by the pronounced dynamic sea level drop in the North Atlantic subpolar gyre in the mid-to-late 2010s, Environ. Res. Lett., 17, 44046, https://doi.org/10.1088/1748-9326/ac5562, 2022a.

675 Wang, S., Wang, Q., Wang, M., Lohmann, G., and Qiao, F.: Arctic Ocean Freshwater in CMIP6 Coupled Models, Earth's Futur., 10, 1–24, https://doi.org/10.1029/2022ef002878, 2022b.

Woodgate, R. A.: Increases in the Pacific inflow to the Arctic from 1990 to 2015, and insights into seasonal trends and driving mechanisms from year-round Bering Strait mooring data, Prog. Oceanogr., 160, 124–154, https://doi.org/10.1016/j.pocean.2017.12.007, 2018a.

680    Woodgate, R. A.: Progress in Oceanography Increases in the Paci fi c in fl ow to the Arctic from 1990 to 2015 , and insights into seasonal trends and driving mechanisms from year-round Bering Strait mooring data, 160, 124–154, https://doi.org/10.1016/j.pocean.2017.12.007, 2018b.

Woodgate, R. A. and Aagaard, K.: Revising the Bering Strait freshwater flux into the Arctic Ocean, Geophys. Res. Lett., 32, 1–4, https://doi.org/10.1029/2004GL021747, 2005.

685    Woodgate, R. A. and Peralta-Ferriz, C.: Warming and Freshening of the Pacific Inflow to the Arctic From 1990-2019 Implying Dramatic Shoaling in Pacific Winter Water Ventilation of the Arctic Water Column, Geophys. Res. Lett., 48, 1–11, https://doi.org/10.1029/2021GL092528, 2021.

Zhang, J. and Steele, M.: Effect of vertical mixing on the Atlantic Water layer circulation in the Arctic Ocean, J. Geophys. Res. Ocean., 112, 1–9, https://doi.org/10.1029/2006JC003732, 2007.

690    Zhang, J., Weijer, W., Steele, M., Cheng, W., Verma, T., and Veneziani, M.: Labrador Sea freshening linked to Beaufort Gyre freshwater release, Nat. Commun., 12, 6–13, https://doi.org/10.1038/s41467-021-21470-3, 2021.

Zweng, M. ., Reagan, J. R., Antonov, J. I., Locarnini, R. A., Mishonov, A. V., Boyer, T. P., Garcia, H. E., Baranova, O. K., Johnson, D. R., Seidov, D., and Biddle, M. M.: NOAA Atlas NESDIS 74 WORLD OCEAN ATLAS 2013 Volume 2 : Salinity, World Ocean Atlas, 2, 182, 2013.
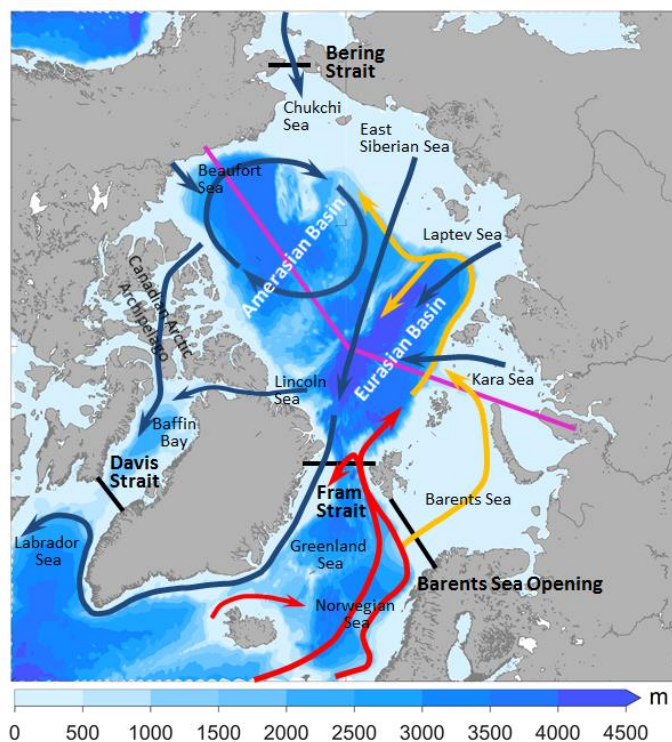
695

**Figure 1. Schematic of main ocean circulations in the pan-Arctic Ocean. The freshwater circulation is shown with dark blue arrows, and the Atlantic Water circulation is shown with red/orange arrows. The black lines indicate the four Arctic gateways used in this study. The pink line along 70 °E and 145 °W crossing the North Pole indicates the location of section S used in Figs. 4, S1, and S2.**
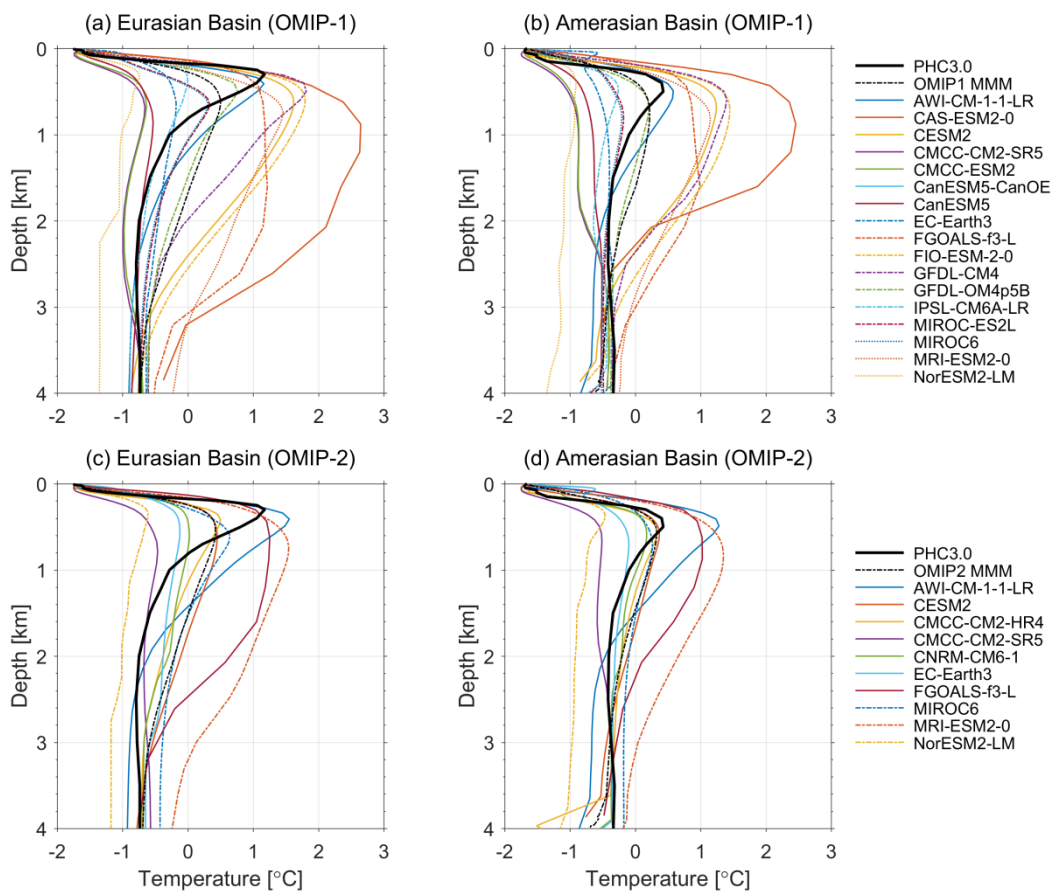
**Figure 2. Potential temperature (unit: ℃) profiles of averaged from 1971 to 2000 in the Eurasian and Amerasian Basins. MMM indicates multi-model mean.**
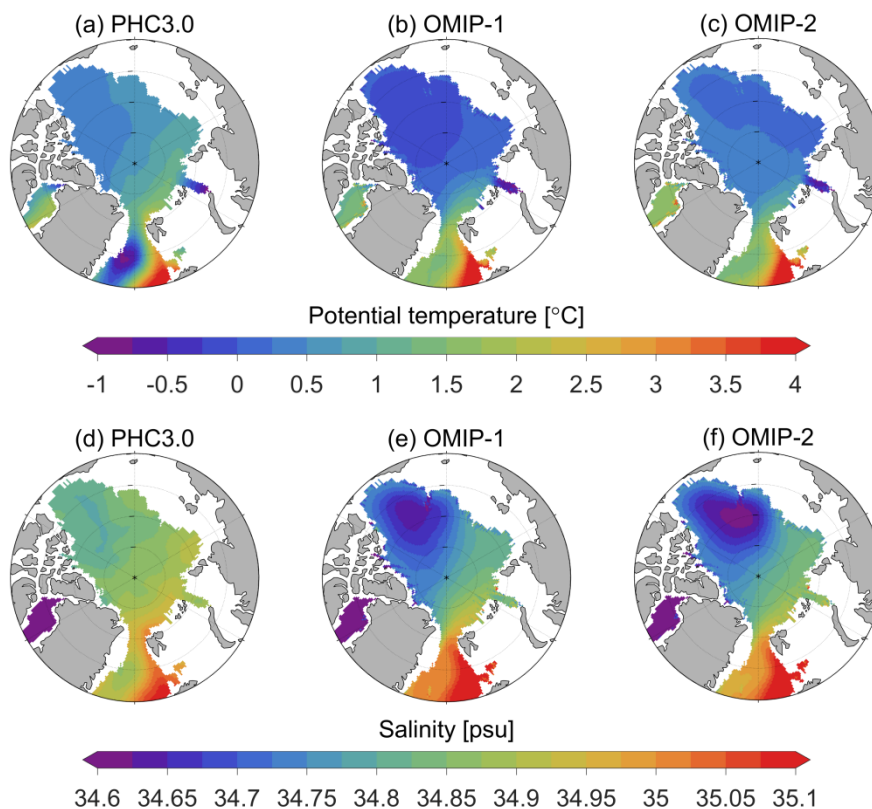
**Figure 3.** (upper) Potential temperature and (bottom) salinity at 400 m from (a,d) PHC3.0, (b,e) OMIP-1, and (c,f) OMIP-2 multi-
705 model mean results. The average over 1971–2000 is shown for OMIP-1 and OMIP-2. The eight models with both OMIP-1 and
OMIP-2 simulations (indicated with bold model ID in Table 1) are used here.
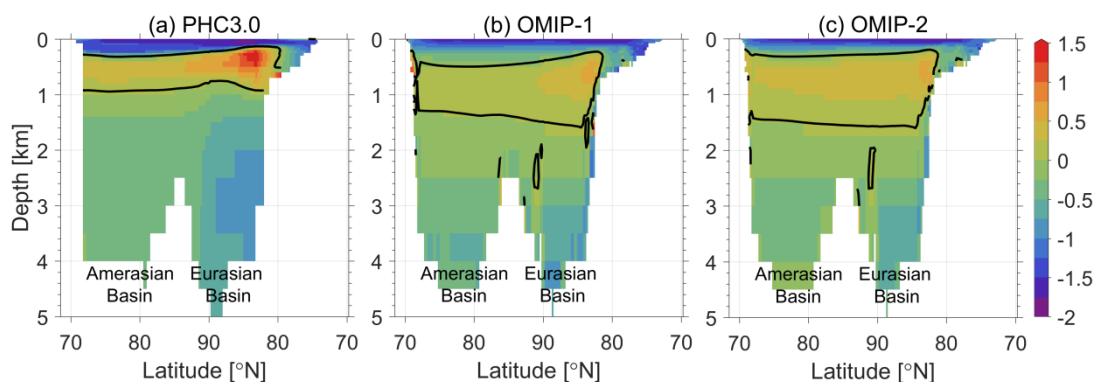
**Figure 4.** Vertical section of potential temperature (unit: ℃) along the 70 ̊E - 145 ̊W section S (indicated in Fig. 1) from the
PHC3.0 dataset, OMIP-1, and OMIP-2 multi-model mean results. The averages over 1971–2000 are shown for the model results.
710 Black line is the 0 ℃ isotherm, which can be considered as the boundary of the Atlantic Water layer. The eight models with bold
model ID in Table 1 are used here.
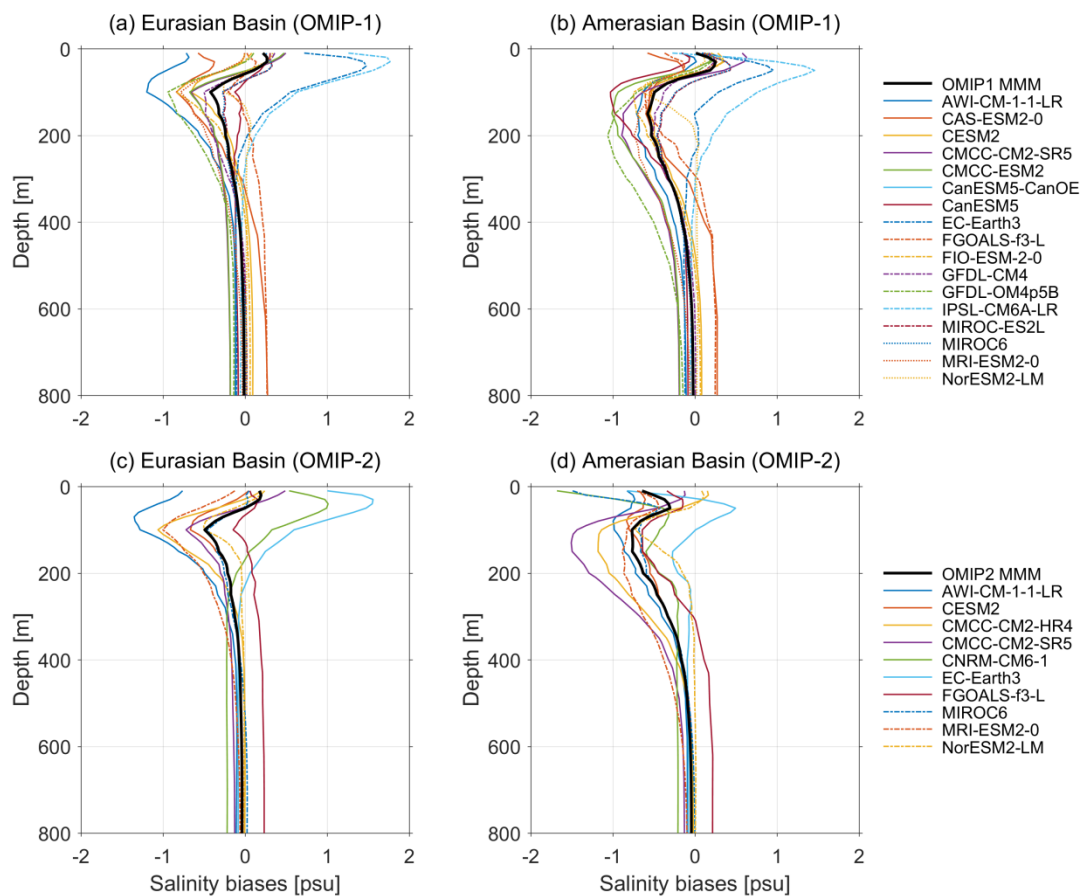
**Figure 5. The basin-mean biases of salinity (unit: psu) in the Eurasian and Amerasian basins. The biases are calculated as the difference between the 1971–2000 model mean and the PHC3.0. MMM indicates multi-model mean.**
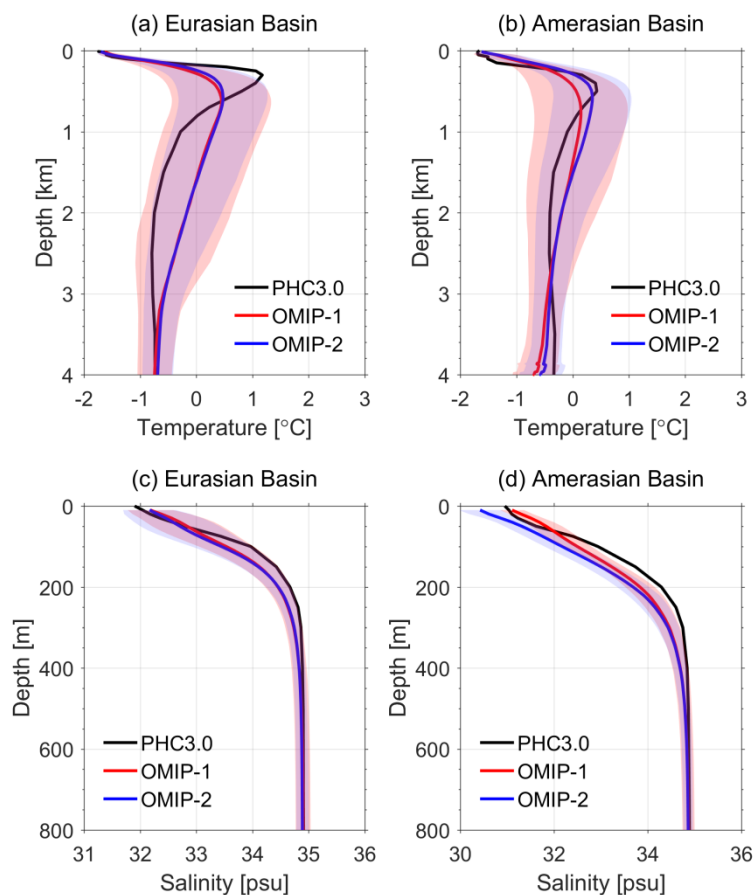
**Figure 6. Multi-model mean (MMM) basin-mean (upper) potential temperature (unit: ℃) and (lower) salinity (unit: psu) averaged from 1971 to 2000 in the Eurasian and Amerasian basins from OMIP-1 and OMIP-2 models. The model spreads (one standard deviation) are shown with shading areas. The eight models with bold model ID in Table 1 are used here.**

715
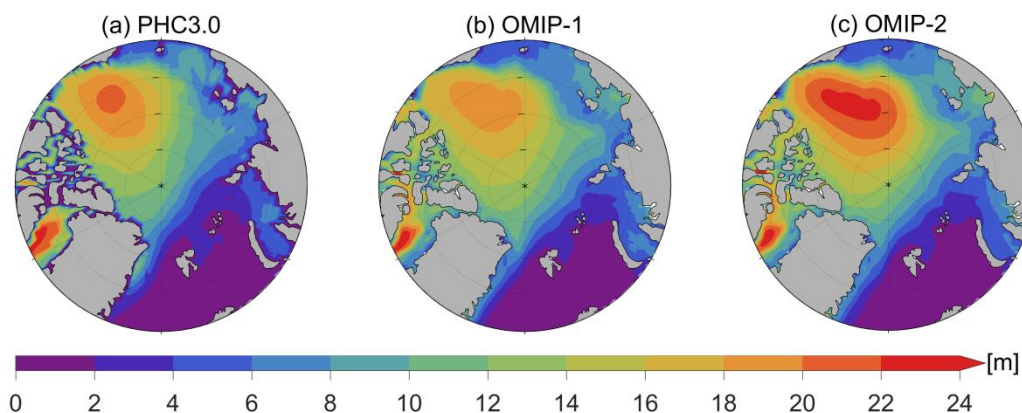
**Figure 7. Liquid freshwater column (m) in (a) PHC3.0, and (b) OMIP-1 and (c) OMIP-2 multi-model mean results. The model results are averaged over 1971–2000. The eight models with bold model ID in Table 1 are used here.**

720
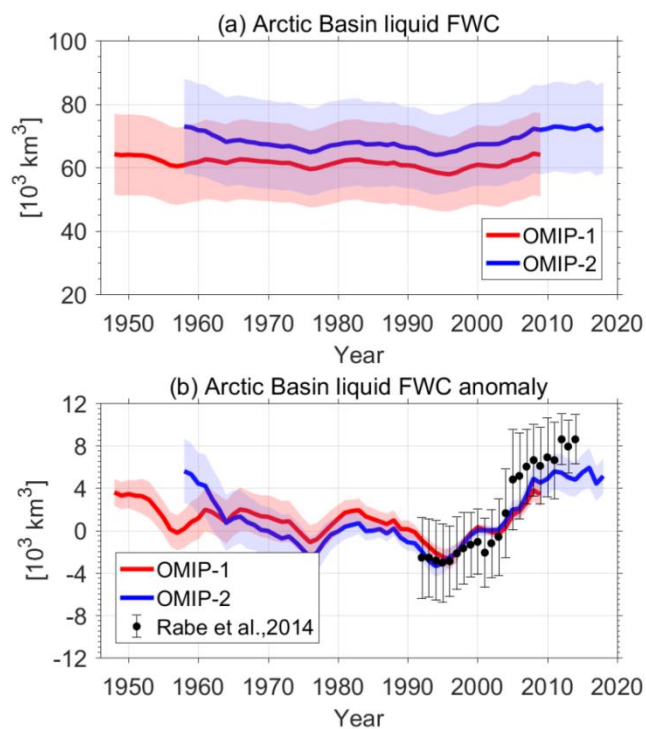
**Figure 8. Liquid freshwater content (FWC) (a) and its anomaly (b) in the Arctic Basin in OMIP-1 (red) and OMIP-2 (blue). The**
725 **lines are the multi-model mean results, and the shading areas represent one standard deviation of the OMIP models. The eight**
**models with bold model ID in Table 1 are used here. Observations are from Rabe et al. (2014) and Wang et al. (2019b).**
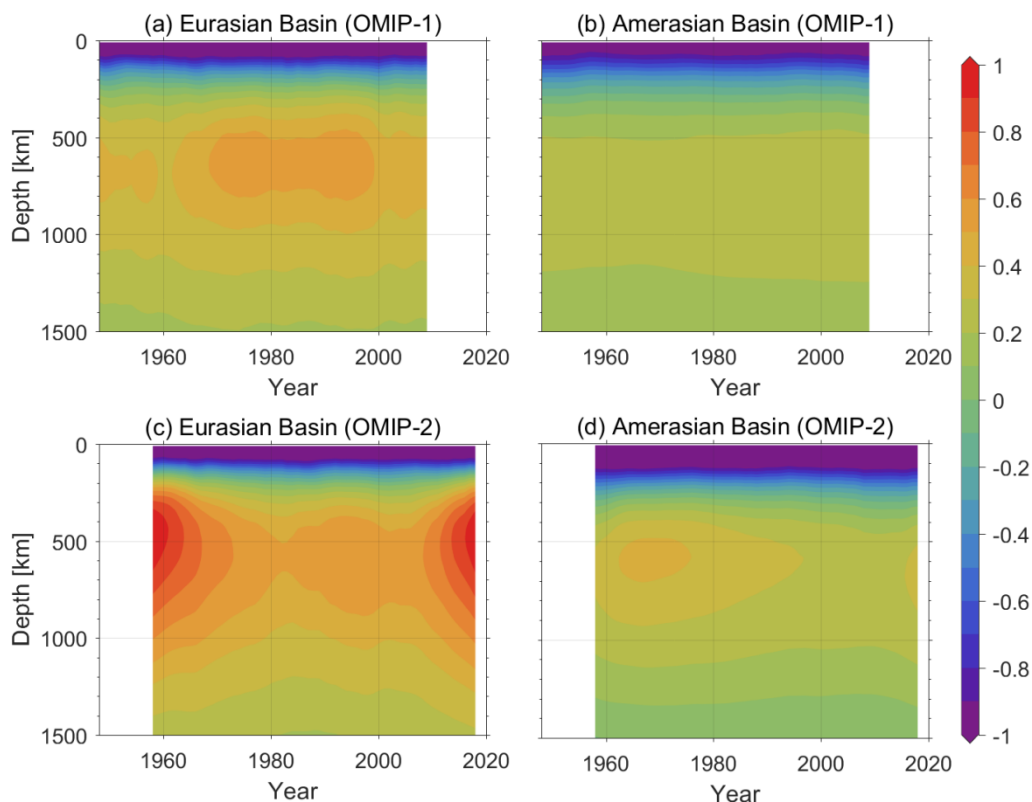
**Figure 9. Hovmöller diagram of basin-mean potential temperature (unit: °C) for the Eurasian Basin (a, c) and Amerasian Basin (b,d) in OMIP-1 (a,b) and OMIP-2 (c, d). The multi-model mean of the eight models with bold model ID in Table 1 are used here.**
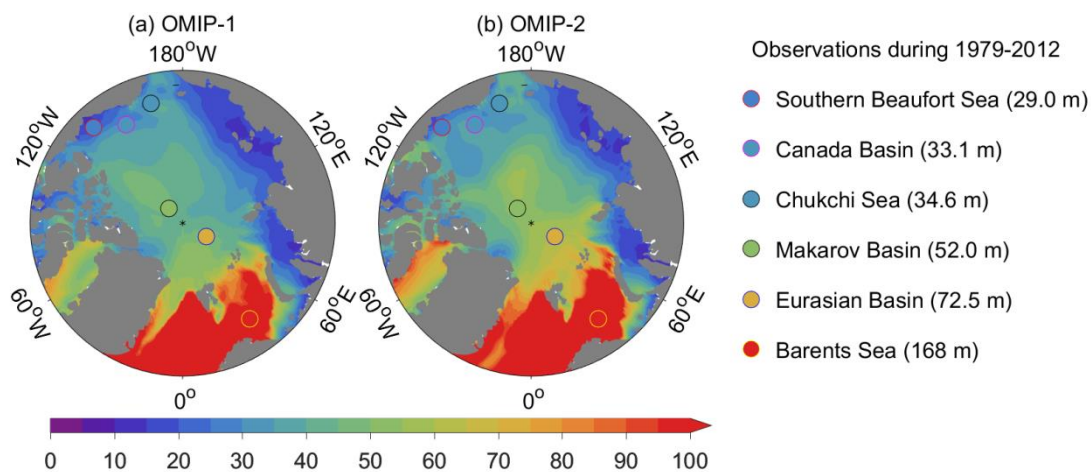
730

**Figure 10. Cold season (November–May) mixed layer depth (unit: m) from OMIP-1 and OMIP-2 multi-model mean results and observations [dots]. The model results are averaged from 1979 to 2009, and the observations are based on the period of 1979 to 2012 (Peralta-Ferriz and Woodgate, 2015). The eight models with bold model ID in Table 1 are used here.**
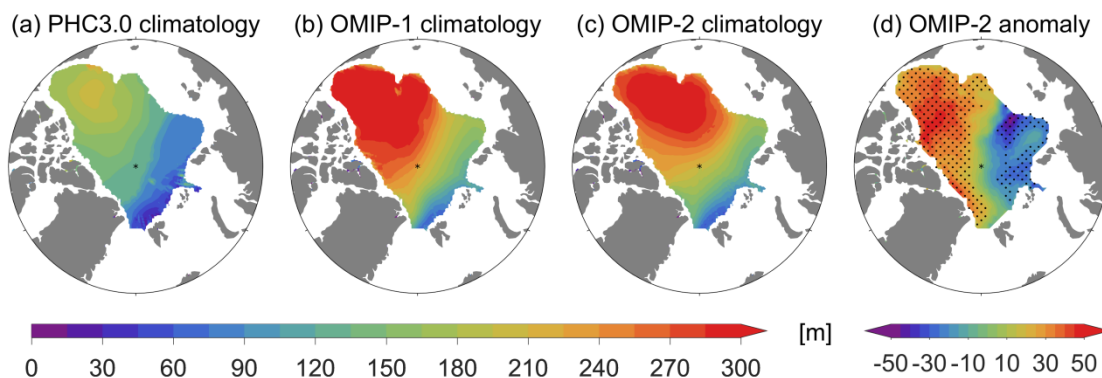
735 **Figure 11. Cold halocline base depth from (a) PHC3.0, (b) OMIP-1 and (c) OMIP-2 multi-model mean results and its anomaly (d) of 2009-2018 relative to 1979-2008 from OMIP-2. The average time period for (b) and (c) is 1971–2000. Dots in (d) indicate that anomaly is larger than variability (one standard deviation of the results from 1979–2008). The eight models with bold model ID in Table 1 are used here.**
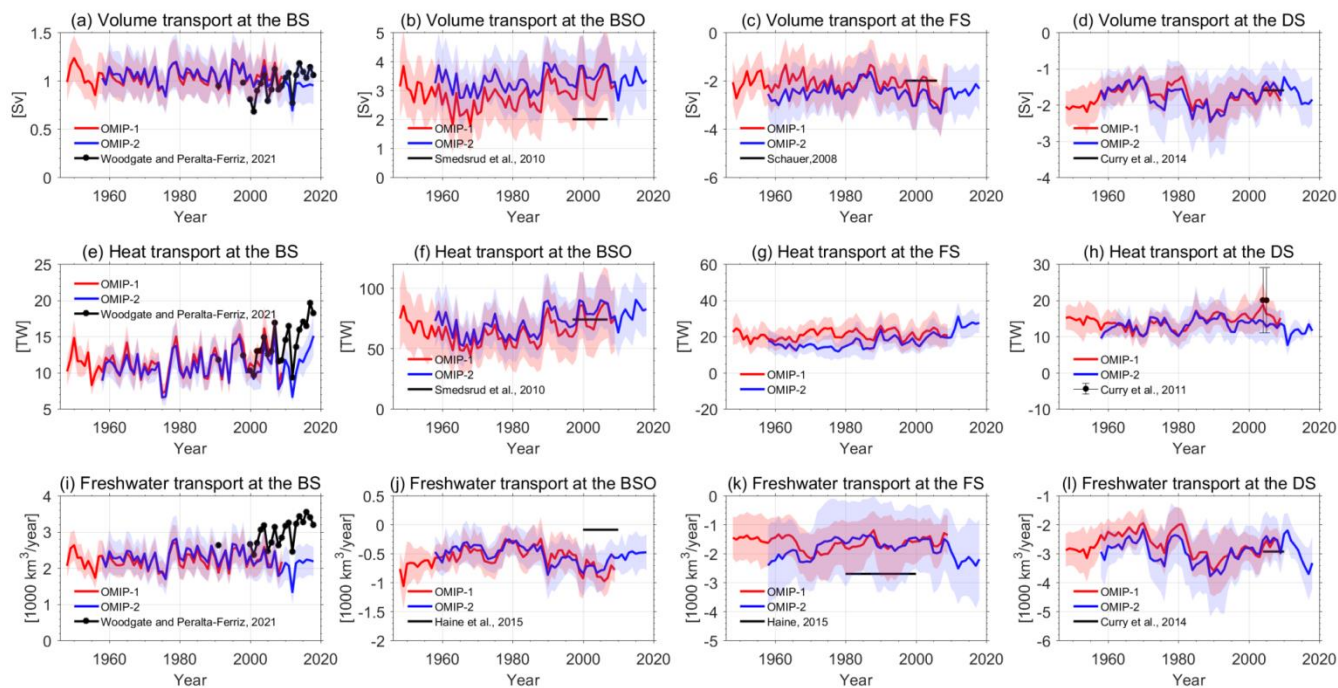
740 **Figure 12. Volume, heat, and liquid freshwater transports through the Bering Strait (BS), Barents Sea Opening (BSO), Fram Strait (FS), and Davis Strait (DS) in OMIP-1 (red), OMIP-2 (blue), and observations (black). The multi-model mean results are shown with lines, and the shading areas represent one standard deviation of the OMIP models. Seven models (AWI-CM-1-1-LR, CESM2, CMCC-CM2-SR5, EC-Earth3, MIROC6, MRI-ESM2-0, and NorESM2-LM) are used here. Ocean heat transport through the Bering Strait is calculated using reference temperature of −1.9 ℃ to be consistent with the observations. Reference**
745 **temperature of 0 ℃ is used for other three gateways.**

**Table 1. Model information. The eight models with bold model ID were used in both OMIP-1 and OMIP-2 simulations. Other models were only available in either OMIP-1 or OMIP-2 simulations.**

| No | Model ID | Sea-ice Model | Ocean Model | Grid Number x × y × z |
|----|----------|---------------|-------------|------------------------|
| 1 | **AWI-CM-1-1-LR** | FESIM2 | FESOM1.4 | 126859 ×46 |
| 2 | CanESM5 | LIM2 | NEMO3.4.1 | 360×291×45 |
| 3 | CanESM5-CanOE | LIM2 | NEMO3.4.1 | 360×291×45 |
| 4 | CAS-ESM2-0 | CICE4 | LICOM2.0 | 360×196×30 |
| 5 | **CESM2** | CICE5.1 | POP2 | 384×320×60 |
| 6 | CMCC-CM2-HR4 | CICE4.0 | NEMO3.6 | 1442×1051×50 |
| 7 | **CMCC-CM2-SR5** | CICE4.0 | NEMO3.6 | 360×291×50 |
| 8 | CMCC-ESM2 | CICE4.0 | NEMO3.6 | 362×292×50 |
| 9 | CNRM-CM6-1 | Gelato 6.1 | NEMO3.6 | 362×294×75 |
| 10 | **EC-Earth3** | LIM3 | NEMO3.6 | 362×292×75 |
| 11 | **FGOALS-f3-L** | CICE4.0 | LICOM3.0 | 360×218×30 |
| 12 | FIO-ESM-2-0 | CICE4.0 | POP2-W | 384×320×60 |
| 13 | GFDL-CM4 | GFDL-SIS2.0 | GFDL-MOM6 | 1440×1080×35 |
| 14 | GFDL-OM4p5B | GFDL-SIS2.0 | GFDL-MOM6 | 720×576×35 |
| 15 | IPSL-CM6A-LR | NEMO-LIM3 | NEMO-OPA | 362×332×75 |
| 16 | **MIROC6** | COCO4.9 | COCO4.9 | 360×256×63 |
| 17 | MIROC-ES2L | COCO4.9 | COCO4.9 | 360×256×63 |
| 18 | **MRI-ESM2-0** | MRI.COM4.4 | MRI.COM4.4 | 360×363×61 |
| 19 | **NorESM2-LM** | CICE5.1 | BLOM | 360×384×53 |

750

755

**Table 2. Mean ocean volume transport and the standard deviation (unit: Sv) through the four Arctic Ocean gateways in OMIP-1. Positive values indicate flux into the Arctic Ocean. The results of last cycle (1948–2009) are used in the analysis.**

| Model | Bering Strait | | Bering Sea Opening | | Fram Strait | | Davis Strait | |
|---|---|---|---|---|---|---|---|---|
| | Mean | STD | Mean | STD | Mean | STD | Mean | STD |
| AWI-CM-1-1-LR | 0.8 | 0.1 | 2.0 | 0.4 | -2.0 | 0.4 | -1.0 | 0.2 |
| CAS-ESM2-0 | 1.1 | 0.1 | 0.3 | 0.3 | -1.3 | 0.3 | 0.0 | 0.0 |
| CESM2 | 0.8 | 0.1 | 1.4 | 0.5 | -0.7 | 0.5 | -1.6 | 0.1 |
| CMCC-CM2-SR5 | 1.1 | 0.1 | 3.9 | 0.6 | -2.9 | 0.7 | -2.0 | 0.5 |
| CMCC-ESM2 | 1.1 | 0.1 | 4.0 | 0.6 | -3.0 | 0.7 | -2.0 | 0.5 |
| CanESM5-CanOE | 0.7 | 0.1 | 4.1 | 0.5 | -3.0 | 0.5 | -1.6 | 0.3 |
| CanESM5 | 0.7 | 0.1 | 4.1 | 0.5 | -3.2 | 0.5 | -1.6 | 0.3 |
| EC-Earth3 | 1.3 | 0.1 | 4.2 | 0.6 | -2.6 | 0.5 | -2.3 | 0.5 |
| FIO-ESM-2-0 | 0.7 | 0.1 | 1.4 | 0.5 | -0.7 | 0.5 | -1.5 | 0.1 |
| IPSL-CM6A-LR | 1.3 | 0.1 | 3.9 | 0.7 | -2.6 | 0.8 | -2.4 | 0.4 |
| MIROC-ES2L | 1.1 | 0.1 | 3.6 | 0.4 | -3.8 | 0.4 | -1.5 | 0.2 |
| MIROC6 | 1.1 | 0.1 | 3.6 | 0.6 | -3.8 | 0.4 | -1.5 | 0.2 |
| MRI-ESM2-0 | 1.3 | 0.1 | 1.9 | 0.4 | -1.5 | 0.5 | -2.2 | 0.4 |
| NorESM2-LM | 0.8 | 0.1 | 2.9 | 0.5 | -1.5 | 0.4 | -1.8 | 0.3 |
| MMM | 1.0 | 0.1 | 3.0 | 0.5 | -2.3 | 0.5 | -1.6 | 0.3 |

760

**Table 3. Mean ocean volume transport and the standard deviation (unit: Sv) through the four Arctic Ocean gateways in OMIP-2. Positive values indicate flux into the Arctic Ocean. The results of last cycle (1958–2018) are used in the analysis.**

| Model | Bering Strait | | Bering Sea Opening | | Fram Strait | | Davis Strait | |
|---|---|---|---|---|---|---|---|---|
| | Mean | STD | Mean | STD | Mean | STD | Mean | STD |
| AWI-CM-1-1-LR | 0.9 | 0.1 | 2.5 | 0.4 | -2.9 | 0.3 | -0.6 | 0.2 |
| CESM2 | 0.7 | 0.1 | 2.0 | 0.4 | -1.3 | 0.3 | -1.5 | 0.2 |
| CMCC-CM2-HR4 | 1.2 | 0.2 | 3.5 | 0.3 | -2.1 | 0.5 | -2.2 | 0.4 |
| CMCC-CM2-SR5 | 1.2 | 0.2 | 4.0 | 0.4 | -2.4 | 0.7 | -2.6 | 0.7 |
| CNRM-CM6-1 | 1.3 | 0.1 | 4.6 | 0.5 | -4.3 | 0.4 | -1.7 | 0.5 |
| EC-Earth3 | 1.4 | 0.1 | 4.4 | 0.4 | -3.1 | 0.5 | -2.4 | 0.5 |
| MIROC6 | 1.2 | 0.1 | 4.4 | 0.4 | -3.9 | 0.3 | -1.4 | 0.2 |
| MRI-ESM2-0 | 1.3 | 0.1 | 2.0 | 0.3 | -1.8 | 0.4 | -1.8 | 0.3 |
| NorESM2-LM | 0.8 | 0.1 | 2.8 | 0.4 | -1.3 | 0.3 | -2.0 | 0.4 |
| MMM | 1.1 | 0.1 | 3.3 | 0.4 | -2.6 | 0.4 | -1.8 | 0.4 |

765

**Table 4. Mean ocean heat transport and the standard deviation (unit: TW) through the four Arctic Ocean gateways in OMIP-1. Positive values indicate flux into the Arctic Ocean. The results of last cycle (1948–2009) are used in the analysis.**

| Model | Bering Strait | | Bering Sea Opening | | Fram Strait | | Davis Strait | |
|---|---|---|---|---|---|---|---|---|
| | Mean | STD | Mean | STD | Mean | STD | Mean | STD |
| AWI-CM-1-1-LR | 2.3 | 1.6 | 62.3 | 8.2 | 24.0 | 7.7 | 15.8 | 5.4 |
| CAS-ESM2-0 | 7.5 | 1.8 | 18.6 | 3.7 | 25.3 | 3.2 | 6.3 | 1.1 |
| CESM2 | 3.6 | 1.4 | 30.2 | 8.1 | 14.1 | 2.8 | 14.6 | 1.4 |
| CMCC-CM2-SR5 | 3.2 | 2.0 | 84.4 | 13.7 | 22.6 | 4.1 | 16.6 | 4.6 |
| CMCC-ESM2 | 3.2 | 2.0 | 88.9 | 14.5 | 24.7 | 5.0 | 14.9 | 4.2 |
| CanESM5-CanOE | 3.4 | 1.4 | 84.1 | 13.5 | 17.3 | 2.4 | 8.9 | 1.4 |
| CanESM5 | 3.4 | 1.4 | 84.1 | 13.5 | 16.6 | 2.2 | 8.9 | 1.4 |
| EC-Earth3 | 2.9 | 2.0 | 90.4 | 15.0 | 12.7 | 3.3 | 11.0 | 2.0 |
| FIO-ESM-2-0 | 3.3 | 1.3 | 29.4 | 8.3 | 14.9 | 3.0 | 14.1 | 1.4 |
| IPSL-CM6A-LR | 2.6 | 2.0 | 83.3 | 16.6 | 20.8 | 6.5 | 13.3 | 2.3 |
| MIROC-ES2L | 3.5 | 1.6 | 86.3 | 12.7 | 29.8 | 3.1 | 11.8 | 2.3 |
| MIROC6 | 3.4 | 1.6 | 89.9 | 16.1 | 30.3 | 3.1 | 11.9 | 2.3 |
| MRI-ESM2-0 | 3.5 | 2.0 | 39.9 | 8.2 | 25.0 | 2.5 | 17.9 | 1.8 |
| NorESM2-LM | 2.7 | 1.1 | 55.5 | 10.5 | 18.3 | 3.2 | 10.8 | 2.0 |
| MMM | 3.5 | 1.7 | 66.2 | 11.6 | 21.2 | 3.7 | 12.6 | 2.4 |

**Table 5. Mean ocean heat transport and the standard deviation (unit: TW) through the four Arctic Ocean gateways in OMIP-2. Positive values indicate flux into the Arctic Ocean. The results of last cycle (1958–2018) are used in the analysis.**

| Model | Bering Strait | | Bering Sea Opening | | Fram Strait | | Davis Strait | |
|---|---|---|---|---|---|---|---|---|
| | Mean | STD | Mean | STD | Mean | STD | Mean | STD |
| AWI-CM-1-1-LR | 2.1 | 1.7 | 69.8 | 8.8 | 22.0 | 8.2 | 14.2 | 4.8 |
| CESM2 | 2.9 | 1.4 | 36.6 | 8.7 | 12.9 | 2.6 | 13.2 | 1.4 |
| CMCC-CM2-HR4 | 5.1 | 2.3 | 85.0 | 10.0 | 39.3 | 14.1 | 23.1 | 5.2 |
| CMCC-CM2-SR5 | 3.8 | 2.2 | 86.9 | 13.7 | 16.9 | 4.6 | 18.3 | 5.5 |
| CNRM-CM6-1 | 1.8 | 2.1 | 103.9 | 17.4 | 13.8 | 4.0 | 7.5 | 2.1 |
| EC-Earth3 | 2.7 | 2.1 | 98.1 | 13.6 | 13.0 | 5.8 | 10.7 | 2.0 |
| MIROC6 | 2.5 | 2.0 | 81.9 | 13.4 | 26.9 | 5.4 | 11.1 | 2.0 |
| MRI-ESM2-0 | 3.4 | 2.1 | 43.5 | 8.5 | 25.7 | 3.5 | 15.5 | 2.4 |
| NorESM2-LM | 2.6 | 1.3 | 59.1 | 10.7 | 14.8 | 5.6 | 10.3 | 2.7 |
| MMM | 3.0 | 1.9 | 73.9 | 11.6 | 20.6 | 6.0 | 13.8 | 3.1 |

**Table 6. Mean freshwater transport and the standard deviation (unit: $10^3$ km$^3$/year) through the four Arctic Ocean gateways in OMIP-1. Positive transports freshen the Arctic Ocean. The results of last cycle (1948–2009) are used in the analysis.**

| Model | Bering Strait | | Bering Sea Opening | | Fram Strait | | Davis Strait | |
|---|---|---|---|---|---|---|---|---|
| | Mean | STD | Mean | STD | Mean | STD | Mean | STD |
| AWI-CM-1-1-LR | 2.0 | 0.3 | -0.5 | 0.2 | -2.6 | 0.5 | -2.2 | 0.5 |
| CAS-ESM2-0 | 2.3 | 0.2 | -0.6 | 0.1 | -3.3 | 0.2 | -0.2 | 0.1 |
| CESM2 | 1.7 | 0.2 | -0.6 | 0.2 | -1.3 | 0.3 | -2.6 | 0.3 |
| CMCC-CM2-SR5 | 2.3 | 0.3 | -0.4 | 0.3 | -1.9 | 0.6 | -3.1 | 0.7 |
| CMCC-ESM2 | 2.4 | 0.3 | -0.3 | 0.3 | -2.2 | 0.7 | -3.2 | 0.7 |
| CanESM5-CanOE | 1.7 | 0.3 | -0.8 | 0.2 | -1.6 | 0.4 | -2.8 | 0.5 |
| CanESM5 | 1.7 | 0.3 | -0.8 | 0.2 | -1.5 | 0.4 | -2.8 | 0.5 |
| EC-Earth3 | 2.8 | 0.3 | -0.3 | 0.3 | -0.5 | 0.3 | -3.0 | 0.7 |
| FIO-ESM-2-0 | 1.5 | 0.2 | -0.5 | 0.1 | -1.4 | 0.3 | -2.6 | 0.2 |
| IPSL-CM6A-LR | 2.7 | 0.4 | -0.5 | 0.3 | -0.3 | 0.2 | -2.7 | 0.6 |
| MIROC-ES2L | 2.3 | 0.2 | -0.6 | 0.3 | -2.4 | 0.3 | -2.3 | 0.4 |
| MIROC6 | 2.3 | 0.2 | -0.5 | 0.3 | -2.4 | 0.2 | -2.3 | 0.4 |
| MRI-ESM2-0 | 2.6 | 0.3 | -0.6 | 0.1 | -2.1 | 0.3 | -3.8 | 0.6 |
| NorESM2-LM | 1.8 | 0.2 | -1.1 | 0.2 | -0.7 | 0.2 | -2.0 | 0.3 |
| MMM | 2.1 | 0.3 | -0.6 | 0.2 | -1.7 | 0.3 | -2.5 | 0.5 |

**Table 7. Mean freshwater transport and the standard deviation (unit: $10^3$ km$^3$/year) through the four Arctic Ocean gateways in OMIP-2. Positive transports freshen the Arctic Ocean. The results of last cycle (1958–2018) are used in the analysis.**

| Model | Bering Strait | | Bering Sea Opening | | Fram Strait | | Davis Strait | |
|---|---|---|---|---|---|---|---|---|
| | Mean | STD | Mean | STD | Mean | STD | Mean | STD |
| AWI-CM-1-1-LR | 2.1 | 0.3 | -0.3 | 0.2 | -4.0 | 0.5 | -1.9 | 0.5 |
| CESM2 | 1.6 | 0.2 | -0.5 | 0.1 | -1.3 | 0.2 | -2.8 | 0.3 |
| CMCC-CM2-HR4 | 2.6 | 0.4 | -0.7 | 0.1 | -2.6 | 0.8 | -3.9 | 0.6 |
| CMCC-CM2-SR5 | 2.5 | 0.4 | -0.6 | 0.2 | -1.5 | 0.8 | -4.4 | 0.9 |
| CNRM-CM6-1 | 3.2 | 0.4 | 0.2 | 0.3 | -3.1 | 1.0 | -4.3 | 1.3 |
| EC-Earth3 | 3.1 | 0.4 | -0.1 | 0.2 | -0.7 | 0.4 | -3.4 | 0.6 |
| MIROC6 | 2.4 | 0.2 | -0.6 | 0.2 | -2.9 | 0.4 | -2.7 | 0.4 |
| MRI-ESM2-0 | 2.5 | 0.3 | -0.6 | 0.1 | -2.8 | 0.4 | -3.7 | 0.6 |
| NorESM2-LM | 1.8 | 0.2 | -1.1 | 0.2 | -0.5 | 0.3 | -2.4 | 0.4 |
| MMM | 2.4 | 0.3 | -0.5 | 0.2 | -2.2 | 0.5 | -3.3 | 0.6 |